

AD-A118 802

STANFORD UNIV CA INFORMATION SYSTEMS LAB  
RESEARCH ON ADAPTIVE ANTENNA TECHNIQUES IV.(U)

F/G 17/4

AUG 61 B WIDROW, K DUVALL, R GOOCH, W NEWMAN N00019-80-C-0483

NL

UNCLASSIFIED

[ OH ]  
AO 3  
118802

END  
DATE  
FORMED  
09-82  
DTIC

AD A118802

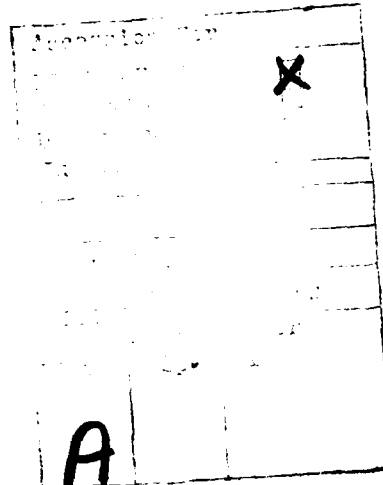
RESEARCH ON ADAPTIVE ANTENNA TECHNIQUES IV

(1)

FINAL REPORT

by

B. Widrow  
K. Duvall  
R. Gooch  
W. Newman



August 1981



Information Systems Laboratory  
Department of Electrical Engineering  
Stanford University  
Stanford, CA 94305

This research was supported by the  
Naval Air Systems Command of the Department of Defense  
under Contract N00019-80-C-0483



E

The views and conclusions contained in this document  
are those of the authors and should not be interpreted as  
necessarily representing the official policies, either expressed or implied  
of the Naval Air Systems Command or the U.S. Government.

APPROVED FOR PUBLIC RELEASE:  
DISTRIBUTION UNLIMITED

82 09 02 034

DMC FILE COPY

## I. INTRODUCTION

All adaptive beamformers utilizing some form of automatic minimization of mean square error exhibit signal cancellation phenomena when adapting rapidly. These effects result from adaptive interaction between signal and interference, when signal and interference are received simultaneously. Similar phenomena have been observed and analyzed in relatively simple adaptive noise cancelling systems. A study of these phenomena in the simpler systems is used to provide insight into similar behavior in adaptive antennas. A method for alleviating signal cancellation has been devised by K. Duvall, whereby the signal components are removed from the adaptive process, then reinserted to form the final system output. B. Widrow has devised a different solution to the problem: to spatially (or electronically) move the receiving array to modulate emanations received off the look direction, without distorting useful signals incident from the look direction. This approach is called "spatial dither," and introduces the additional possibility of modulating "smart" jammer signals, thereby limiting their effectiveness.

Adaptive antennas have been under development in various forms for the past two decades or so. Although adaptive antennas have been used only in small numbers thus far, they have proven themselves capable of rejecting jamming signals more efficiently than any other known method. Most high performance radar and communications systems being designed for jamming environments will incorporate adaptive antennas. The simultaneous development of spread spectrum techniques and adaptive antennas provides a formidable set of technologies for jam-resistant systems. These technologies are compatible and are frequently used in the same system. An adaptive antenna is used to attenuate strong jamming signals as they appear at the receiver "front end;" spread spectrum techniques are used to neutralize large numbers of weak jammers that may not be eliminated totally by the adaptive antenna.

APPROVED FOR PUBLIC RELEASE  
DISTRIBUTION UNLIMITED

We are now faced with the fact that under certain circumstances jammers can be devised specifically to elude adaptive antennas. This paper is concerned with jamming signals that can potentially defeat or partially defeat known adaptive antenna algorithms. The existence of jammers capable of troubling known adaptive arrays motivates us to develop new adaptive signal processing and array processing algorithms, two of which are proposed herein.

The goals of this paper are three:

- (a) To examine signal cancellation phenomena in adaptive beamformers,
- (b) To formulate approaches toward the elimination of adaptive signal cancellation phenomena,
- (c) To introduce spatial dither algorithms to combat signal cancellation and break up "smart" jammer signals at the receiving array.

## II. SIGNAL CANCELLATION JAMMING

Any adaptive beamformer -- the Howells-Applebaum sidelobe canceller [1,2,3], Widrow's beamformer [4], Griffith's beamformer [5], Frost's beamformer [6], Zahm's beamformer [7], Compton's beamformer [8,9] or combinations and variations of these [10,11], -- is susceptible to attack by simple jammers that may be bandpass noise, a sinusoid, or a sum of sinusoids suitably spaced in frequency. The interaction of such jammers with the desired signal in these adaptive algorithms may cause cancellation of signal components, even when the adaptive beamformers are working perfectly.

To understand how this occurs, consider the Frost beamformer which functions in the following manner. A beam is formed toward a user-selected "look direction." The receiving sensitivity in this direction is then constrained. A typical constraint is one that forces the array to have a unit gain magnitude and zero phase over a selected

passband of frequencies in the look direction. The beamformer is adapted, i.e., its weights are varied to minimize its output power, subject to the constraint which sustains the beam in the look direction. Adaptation subject to the constraint allows the array to accept a signal with gain one if this signal arrives from the look direction; and causes any other signals, e.g., jammer signals, to be rejected as well as possible (in the minimum-total-power sense) as long as they do not arrive from the look direction. Other adaptive beamformers behave similarly with the following exception: the Frost algorithm imposes a "hard" constraint on the signal gain in the look direction; the Widrow and Griffiths beamformers create "soft" constraints in this direction; the Howells-Applebaum and Zahm beamformers apply soft constraints omnidirectionally rather than in the look direction.

Suppose that the Frost beamformer has a sinusoidal input signal arriving from the look direction. This signal should appear at the beamformer output, going through a unit gain. Now suppose a jammer is turned on -- a very strong sinusoidal jammer at the same frequency as the signal, but arriving off the look direction. The jamming sinusoid would normally be rejected by the adaptive beamformer if the signal were not present. With the signal present, however, minimizing the total output power will cause the jammer to be admitted with just the right magnitude and phase to cancel the sinusoidal signal. Thus the signal sinusoid is admitted with a gain of one. On the other hand, just a trickle of the powerful jammer sinusoid is admitted to perfectly cancel the signal sinusoid and produce a net output of zero. The output power is minimized and the constraint is preserved, as it should be with a perfectly working Frost beamformer. But the signal is lost in the process. This amounts to *jamming by signal cancellation*, rather than *jamming by overwhelming the signal with interference*.

If the input signal in the look direction is broadband (rather than sinusoidal) and

the jammer is sinusoidal, the adaptive algorithm will modulate the sinusoidal jammer so that it will cancel some signal components at the jammer frequency and at neighboring frequencies. If the jammer signal contains a sum of sinusoids at spaced frequencies within the passband, the output signal spectrum will be notched at each of the jammer frequencies. This phenomenon could be troublesome for bandpass and spread-spectrum communications.

Similar signal cancellation phenomena have been observed and analyzed in the context of adaptive noise cancelling systems, much simpler systems than adaptive beamformers. A brief discussion and analysis of adaptive noise cancelling follows.

### III. ADAPTIVE NOISE CANCELLING

An adaptive noise canceller is shown in Fig. 1. In the terminology of that field, the "primary input" contains a useful signal  $s$ , plus interference  $n_p$ . The "reference input" is separately obtained in practical systems. It contains interference  $n_r$ , related to the interference of the primary input. Generally the relationship between the two interferences is unknown *a priori*. The adaptive filter shapes the reference interference to replicate the primary interference (in the least-squared-error sense) so that subtraction will remove the interference from the primary input, providing a much more useful output. It has been shown in [12] that an adaptive filter that minimizes output power in the system shown in Fig. 1 causes the system output to be a best least-squares estimate of the useful signal  $s$ . Basically, the Howells-Applebaum sidelobe canceller functions on the same principle, although in certain ways it is considerably more complicated: useful signals and jammer signals appear at both primary and reference inputs; and spatial processing, i.e. array processing, is also involved.

If the reference input is a sinusoid, as shown in Fig. 2, then the signal flow path from primary input to the output behaves like a sharp, linear, time-invariant notch

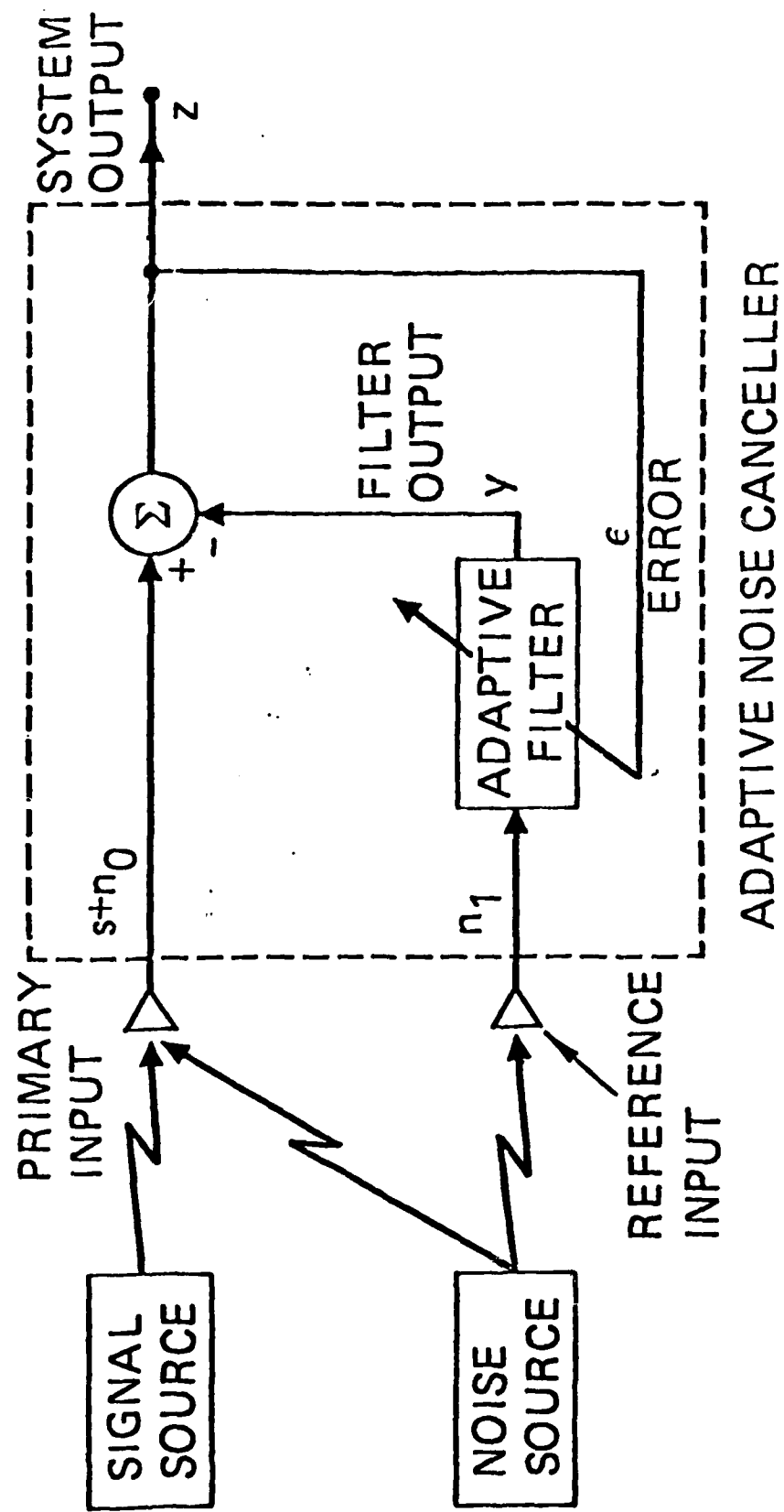
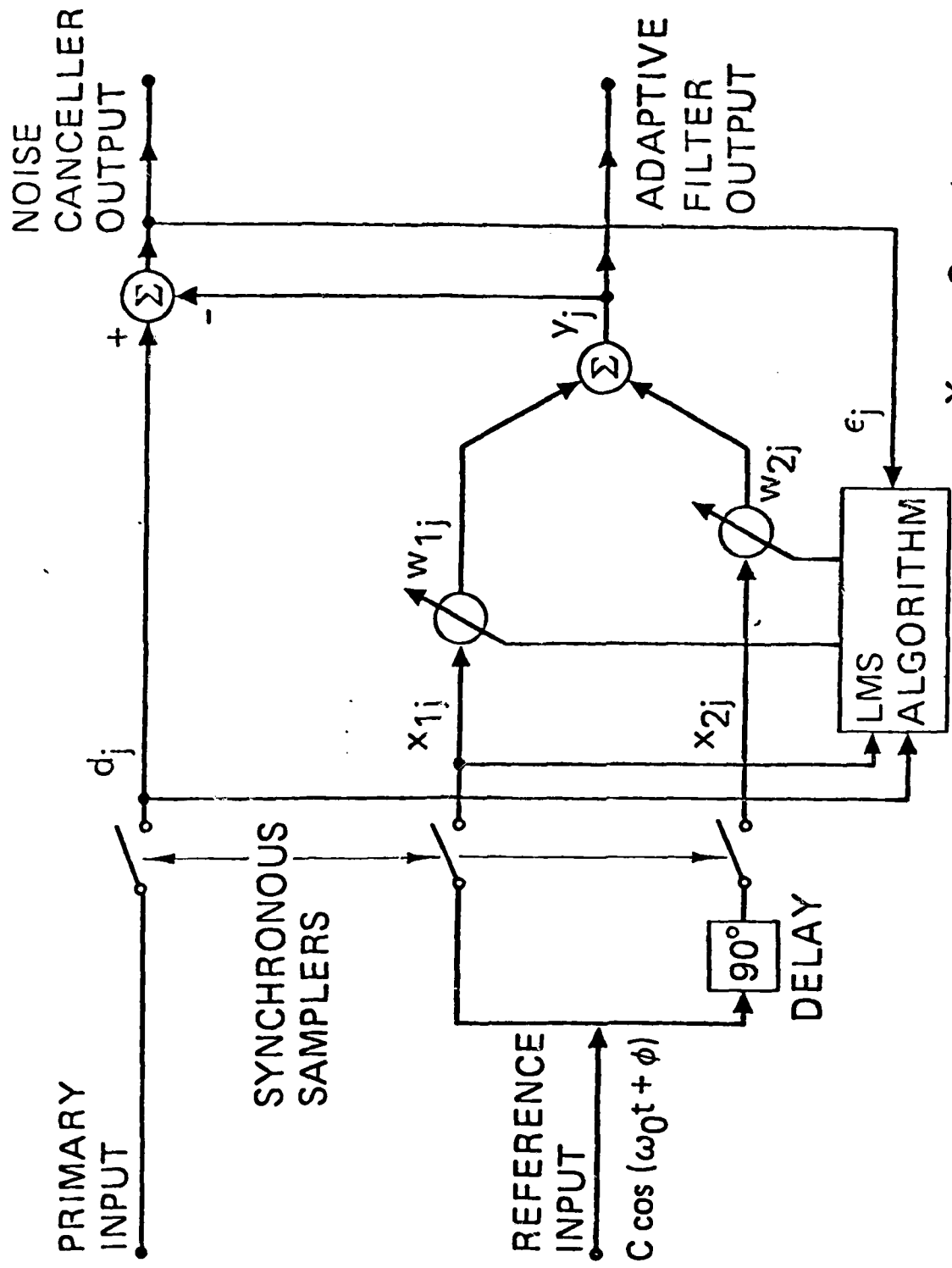


Fig. 1. The adaptive noise cancelling concept.



$$X_{1j} = C \cos(\omega_0 j T + \phi)$$

$$X_{2j} = C \sin(\omega_0 j T + \phi)$$

SAMPLING PERIOD =  $T$  SEC

SAMPLING FREQ.  $\Omega = \frac{2\pi}{T}$  RAD/SEC

Fig. 2. Two-weight noise canceller.

filter. This discovery came as a surprise because the adaptive filter itself is intrinsically nonlinear and time variable. An analysis by John Glover of the notch filter effect was presented in a 1975 Proceedings of IEEE paper by Widrow et al. on the subject of adaptive noise cancelling [12]. A more detailed analysis is contained in Glover's Ph.D. thesis entitled "Adaptive Noise Cancelling of Sinusoidal Interferences," Department of Electrical Engineering, Stanford University, 1975 [13]. A published work based on Glover's thesis has since appeared [14], treating both single and multiple notch cases. Analysis of the simplest case, a single notch created by a two-weight adaptive filter, is outlined below.

#### IV. AN ADAPTIVE NOTCH FILTER

Figure 2 shows an adaptive noise canceller with two adaptive weights. The primary input is assumed to be an arbitrary signal; it could be stochastic, deterministic, periodic, transient, etc. The reference input is assumed to be a pure cosine wave,  $C \cos(\omega_r t + \phi)$ . The primary and reference inputs are sampled at the frequency  $\Omega = 2\pi/T$  rad/s. The reference input is sampled directly, giving  $z_{1j}$ . After undergoing a 90° phase shift, it is sampled again, giving  $z_{2j}$ . The samplers are synchronous and strobe at  $t = 0, T, 2T$ , etc.

A transfer function for the noise canceller shown in Fig. 2 can be obtained by analyzing signal propagation from the primary input to the system output.\* Weight updating in the system is carried out according to the LMS algorithm [15,16]:

$$w_{1j+1} = w_{1j} + 2\mu\epsilon_j z_{1j}$$

$$w_{2j+1} = w_{2j} + 2\mu\epsilon_j z_{2j}. \quad (1)$$

\*It is not obvious, from inspection of Fig. 2, that a transfer function for this propagation path in fact exists. Its existence is shown, however, by the subsequent analysis.

The subscripts indicate the time index;  $\mu$  is a constant controlling the rate of adaptation. Referring to Fig. 3, the sampled reference inputs are

$$x_{1j} = C \cos(\omega_0 jT + \phi). \quad (2)$$

and

$$x_{2j} = C \sin(\omega_0 jT + \phi). \quad (3)$$

The first step in the analysis is to obtain the isolated impulse response from the error  $\epsilon_j$ , point  $C$ , to the filter output, point  $G$ , with the feedback loop from point  $G$  to point  $B$  broken. Let an impulse of amplitude  $\alpha$  be applied at point  $C$  at discrete time  $j = k$ ; that is,

$$\epsilon_j = \alpha \delta(j-k). \quad (4)$$

The  $\delta(j-k)$  is a Kronecker delta function, defined as

$$\delta(j-k) = \begin{cases} 1, & \text{for } j = k \\ 0, & \text{otherwise.} \end{cases} \quad (5)$$

The impulse causes a response at point  $D$  of

$$\epsilon_j x_{1j} = \begin{cases} \alpha C \cos(\omega_0 kT + \phi), & \text{for } j = k \\ 0, & \text{otherwise,} \end{cases} \quad (6)$$

which is the input impulse scaled in amplitude by the instantaneous value of  $x_{1j}$  at  $j = k$ . The signal flow path from point  $D$  to point  $E$  is that of a digital integrator with transfer function  $2\mu/(z-1)$  and impulse response  $2\mu u(j-1)$ , where  $u(j)$  is the discrete unit step function

$$u(j) = \begin{cases} 0, & \text{for } j < 0 \\ 1, & \text{for } j \geq 0. \end{cases} \quad (7)$$

Convolving  $2\mu u(j-1)$  with  $\epsilon_j x_{1j}$  yields a response at point  $E$  of

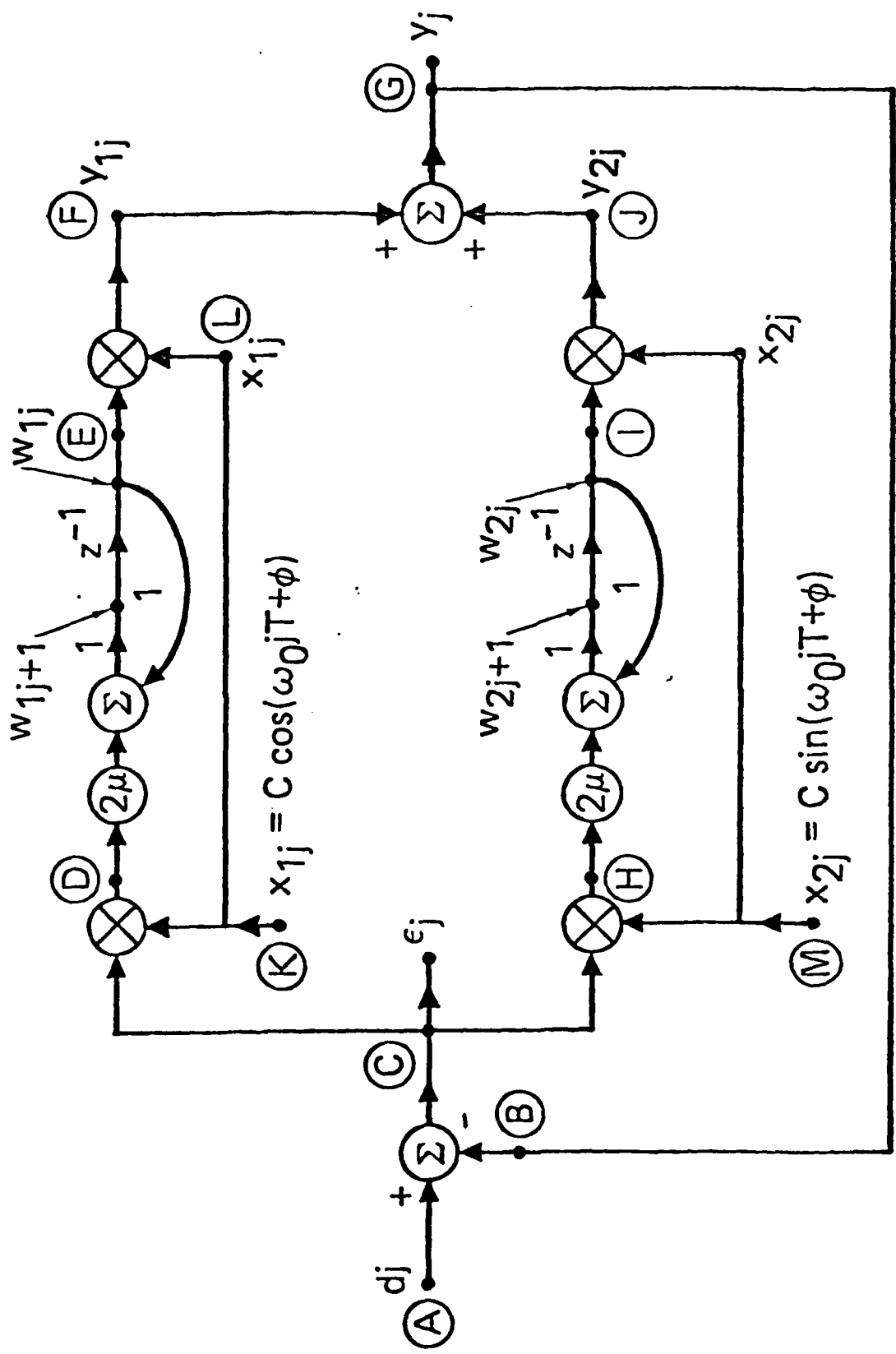


Fig. 3. Flow diagram showing signal propagation in a two-weight adaptive noise canceller.

$$w_{1j} = 2\mu\alpha C \cos(\omega_0 kT + \phi), \quad (8)$$

where  $j \geq k + 1$ . When the scaled and delayed step function is multiplied by  $x_{1j}$ , the response at point F is obtained as

$$y_{1j} = 2\mu\alpha C^2 \cos(\omega_0 jT + \phi) \cos(\omega_0 kT + \phi), \quad (9)$$

where  $j \geq k + 1$ . The corresponding response at point J, obtained in a similar manner, is

$$y_{2j} = 2\mu\alpha C^2 \sin(\omega_0 jT + \phi) \sin(\omega_0 kT + \phi), \quad (10)$$

where  $j \geq k + 1$ . Combining (9) and (10) yields the response at the filter output, point G:

$$\begin{aligned} y_j &= 2\mu\alpha C^2 \cos(\omega_0 T(j-k)) \\ &= 2\mu\alpha C^2 u(j-k-1) \cos(\omega_0 T(j-k)). \end{aligned} \quad (11)$$

Observe that (11) is a function only of  $(j-k)$  and is thus a time invariant impulse response, proportional to the input impulse.

A linear transfer function for the noise canceller can now be derived in the following manner. If the time  $k$  is set equal to zero, the unit impulse response of the linear time-invariant signal-flow path from point C to point G is

$$y_j = 2\mu C^2 u(j-1) \cos(\omega_0 jT), \quad (12)$$

and the transfer function of this path is

$$\begin{aligned} G(z) &= 2\mu C^2 \left[ \frac{z(z - \cos\omega_0 T)}{z^2 - 2z \cos\omega_0 T + 1} - 1 \right] \\ &= \frac{2\mu C^2 (z \cos\omega_0 T - 1)}{z^2 - 2z \cos\omega_0 T + 1}. \end{aligned} \quad (13)$$

This function can be expressed in terms of a radian sampling frequency  $\Omega = 2\pi/T$  as

$$G(z) = \frac{2\mu C^2 |z \cos(2\pi\omega_0 \Omega^{-1}) - 1|}{z^2 - 2z \cos\omega_0 T + 1}. \quad (14)$$

If the feedback loop from point *G* to point *B* is now closed, the transfer function  $H(z)$  from the primary input, point *A*, to the noise canceller output, point *C*, can be obtained from the feedback formula:

$$H(z) = \frac{z^2 - 2z \cos(2\pi\omega_r\Omega^{-1}) + 1}{z^2 - 2(1-\mu C^2)z \cos(2\pi\omega_r\Omega^{-1}) + 1 - 2\mu C^2} \quad (15)$$

Equation (15) shows that the noise canceller with a cosine reference input has the properties of a notch filter at the reference frequency  $\omega_r$  along the signal flow path from primary input to output. The zeros of the transfer function are located in the *Z* plane at

$$z = \exp(\pm i2\pi\omega_r\Omega^{-1}) \quad (16)$$

and are precisely on the unit circle at angles of  $\pm 2\pi\omega_r\Omega^{-1}$  rad. The poles are located at

$$z = (1-\mu C^2)\cos(2\pi\omega_r\Omega^{-1}) \pm i[(1-2\mu C^2) - (1-\mu C^2)\cos^2(2\pi\omega_r\Omega^{-1})]^{1/2}. \quad (17)$$

The poles are inside the unit circle at a radial distance  $(1-2\mu C^2)^{1/2}$ , approximately equal to  $1-\mu C^2$ , from the origin at angles of

$$\pm \arccos[(1-\mu C^2)(1-2\mu C^2)^{-1/2} \cos(2\pi\mu\Omega^{-1})].$$

For slow adaptation, i.e., small values of  $\mu C^2$  these angles depend on the factor

$$\begin{aligned} \frac{1-\mu C^2}{(1-2\mu C^2)^{1/2}} &= \left( \frac{1-2\mu C^2 + \mu^2 C^4}{1-2\mu C^2} \right)^{1/2} \\ &= (1-\mu^2 C^4 + \dots)^{1/2} \\ &\approx 1 - \frac{1}{2}\mu^2 C^4 \end{aligned} \quad (18)$$

which differs only slightly from a value of one. The result is that, in practical instances, the angles of the poles are almost identical to the angles of the zeros.

Figure 4 shows the location of the poles and zeros, and the magnitude of the transfer function in terms of frequency. Since the zeros lie on the unit circle, the depth of the notch in the transfer function is infinite at the frequency  $\omega = \omega_0$ . The sharpness of the notch is determined by the closeness of the poles to the zeros. Corresponding poles and zeros are separated by a distance approximately equal to  $\mu C^2$ . The arc length along the unit circle, centered at the position of a zero, spanning the distance between half-power points, is approximately  $2\mu C^2$ . This length corresponds to a notch bandwidth of

$$\begin{aligned} (BW) &= \mu C^2 \Omega / \pi \\ &= 2\mu C^2 F \text{ Hz}, \end{aligned} \quad (19)$$

where  $F$  is the sampling frequency in Hz. The  $Q$  of the notch is determined by the ratio of the center frequency to the bandwidth,

$$Q \approx \frac{\omega_0 \pi}{\mu C^2 \Omega}. \quad (20)$$

The time constant of the mean square error "learning curve" for the LMS algorithm has been shown to be [7,14].

$$\tau_{mse} = \frac{n}{4\mu \text{ trace } R} \text{ iterations}, \quad (21)$$

where  $R$  is the covariance matrix of the inputs to the weights, and  $n$  is the number of weights. Formula (21) applies when the eigenvalues are all equal. This is the case for the system shown in Fig. 2. Multiplying by the sampling period  $T$ , the time constant is expressed in seconds of real time as

$$\tau_{mse} = \frac{nT}{4\mu \text{ trace } R} \text{ sec.} \quad (22)$$

For the two-weight adaptive filter shown in Fig. 2,

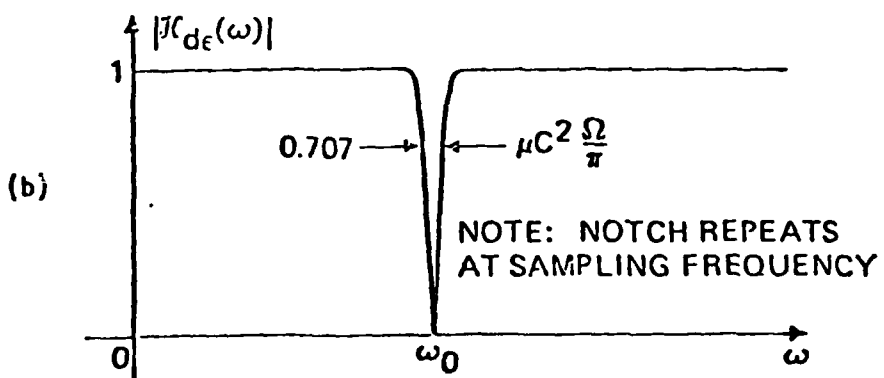
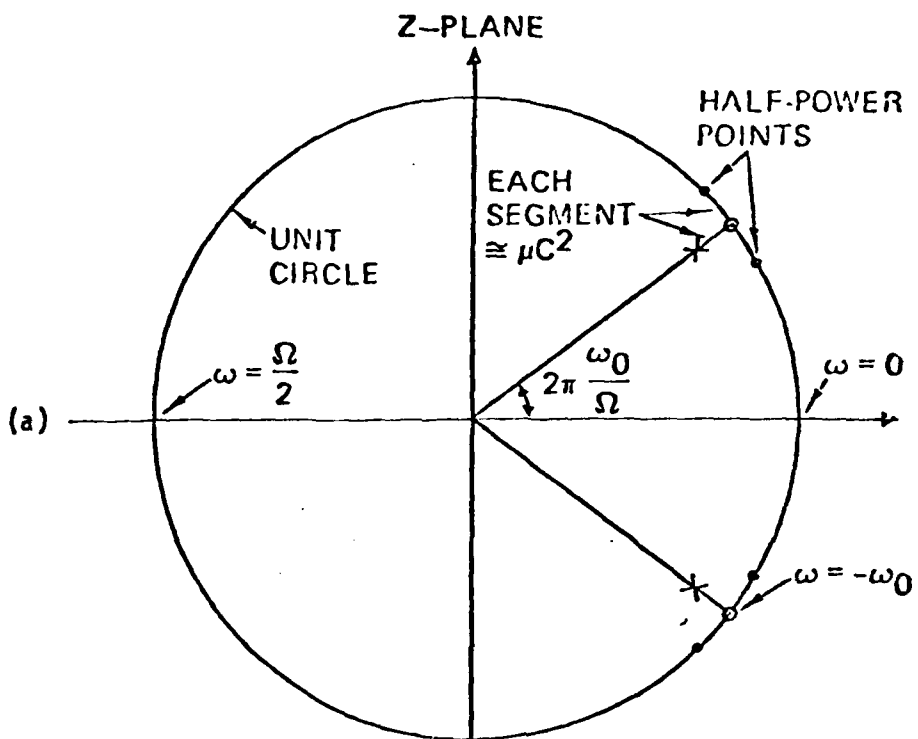


Fig. 4. Properties of transfer function of two-weight adaptive noise canceller. (a) Location of poles and zeros. (b) Magnitude of transfer function.

$$\begin{aligned} \text{trace } R &= \frac{1}{2} C^2 + \frac{1}{2} C^2 \\ &= C^2. \end{aligned} \quad (23)$$

This is the sum of the power into the weights. Combining equations (23), (22), and (19) yields

$$(BW) = \frac{1}{r_{mc}} \text{ Hz.} \quad (24)$$

Thus the bandwidth of the notch is the reciprocal of the time constant of the learning process, for the simple system shown in Fig. 2.

Figure 5 shows the results of two experiments performed to demonstrate the adaptive systems notch-filter behavior. In the first experiment, the primary input was a cosine wave of unit power stepped at 512 discrete frequencies. The reference input was a cosine wave with frequency  $\omega_r$  of  $\pi/2T$  rad/s. The value of  $C$  was 1, and the value of  $\mu$  was  $1.25 \times 10^{-2}$ . The spectra of Fig. 5 were computed by 512 bin Fourier transforms. The output power at each frequency is shown in Fig. 5(a). As the primary frequency approaches the reference frequency, significant cancellation occurs. The weights do not converge to stable values but instead they "tumble" at the difference frequency,\* and the adaptive filter behaves like a modulator, converting the reference frequency into the primary frequency. The theoretical notch width between half-power points,  $1.59 \times 10^{-2} \omega_r$ , compares closely with the measured notch width of  $1.62 \times 10^{-2} \omega_r$ .

In the second experiment, the primary input was composed of uncorrelated samples of white noise of unit power. The reference input and the processing parameters were the same as in the first experiment. An ensemble average of 4096 power spectra at the noise canceller output is shown in Fig. 5(b). An infinite null was not observed in this

\*When the primary and reference frequencies are held at a constant difference, the weights develop a sinusoidal steady state at the difference frequency. In other words, they converge on a dynamic rather than a static solution.

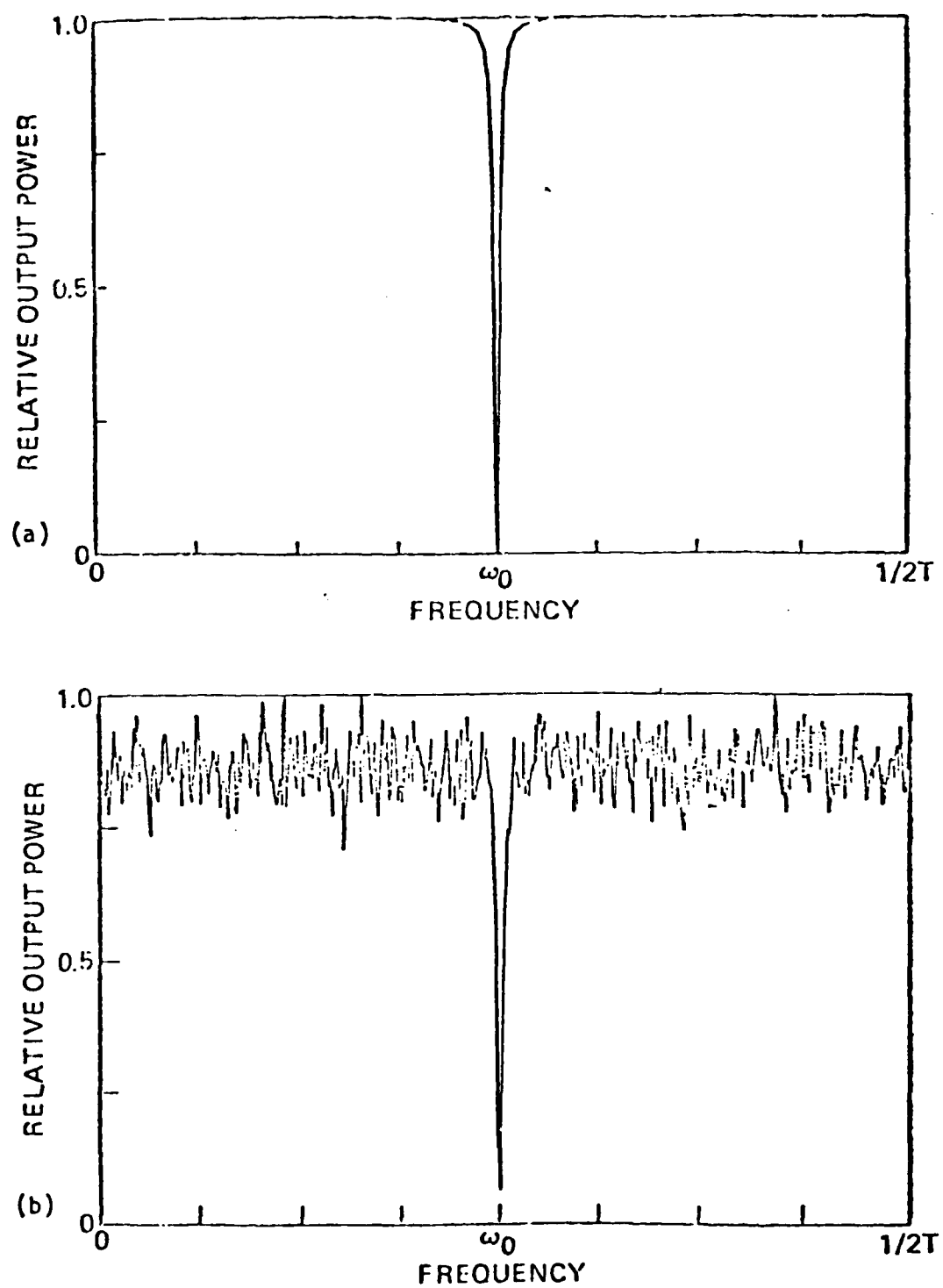


Fig. 5. Results of two-weight adaptive noise cancelling experiments.  
(a) Primary input composed of cosine wave at 512 discrete frequencies. (b) Primary input composed of uncorrelated samples of white noise.

experiment because of the finite frequency resolution of the spectral analysis algorithm.

In these experiments, the filtering of a reference cosine wave of a given frequency cancelled primary input components at adjacent frequencies. This result indicates that, under some circumstances, primary input components may be partially cancelled and distorted even though they are not correlated with the reference input. In practice, this kind of cancellation is significant only when the adaptive process is rapid; that is, when it is effected with large values of  $\mu$ . When the adaptive process is slow, the weights converge to values that are nearly fixed, close to the Wiener solution, and though signal cancellation (as described in this section) occurs, it is generally not significant since the notch is extremely narrow. In any event, the primary input appears at the output having gone through a notch filter.

#### V. SIGNAL CANCELLATION PHENOMENA IN HOWELLS-APPLEBAUM SIDELOBE CANCELLERS

Figure 6 shows a simple form of Howells-Applebaum sidelobe canceller operating in an environment consisting of a signal plus a single jammer. The two antenna elements are omnidirectional, and both antenna elements receive emanations from the signal source *S* and the jammer *J*. Assume that the jammer power is very much greater than the signal power, and that the number of degrees of freedom in the adaptive filter is sufficient to cancel the jammer but not sufficient to cancel both the jammer and the signal. Since the jammer is far more powerful than the signal, it will "grab" the degrees of freedom to effect its own cancellation. The signal will have little influence on the adaptive weights, in accord with Wiener filter theory, and will appear at the system output together with certain small uncancelled jammer components.

The system shown in Figure 6 is similar to the adaptive noise canceller pictured in Fig. 1, except that the reference input in Fig. 6 contains signal along with strong jammer inputs. After the weights have converged to the Wiener solution, the adaptive filter

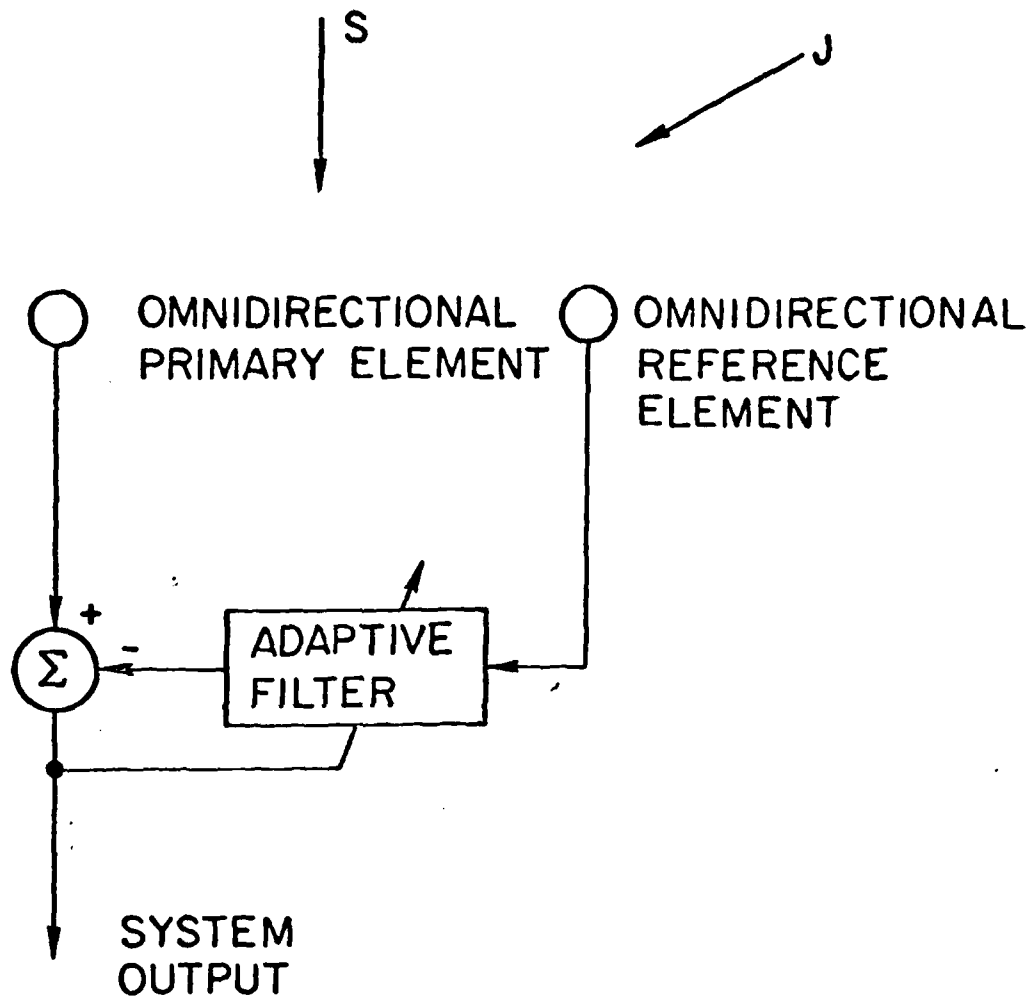


Fig. 6. A simple form of the Howells-Applebaum sidelobe canceller.

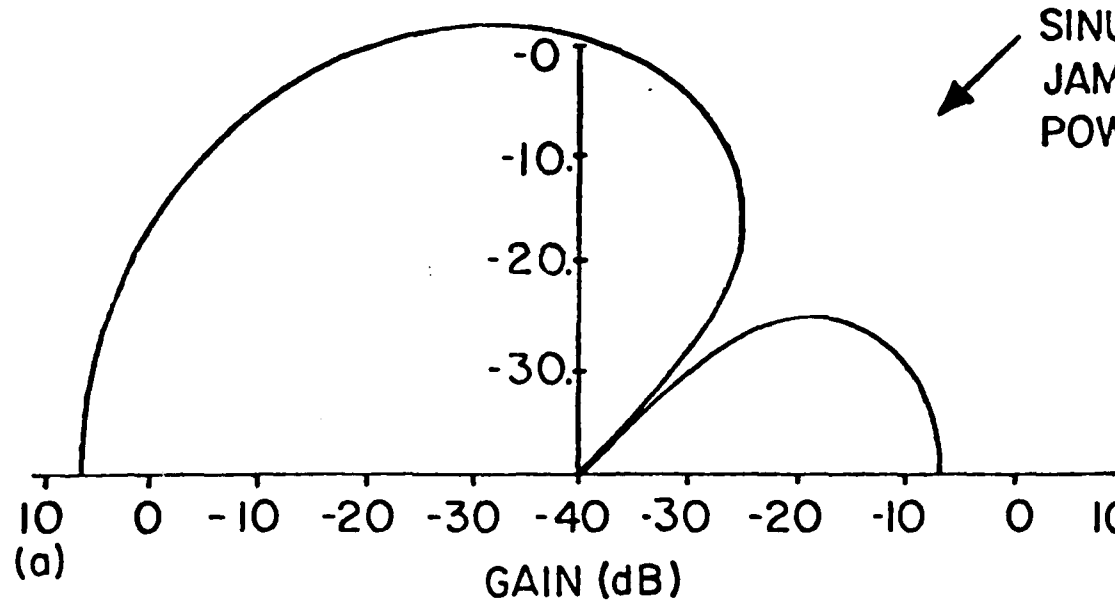
will pass this signal and subtract the result from the primary signal, thereby introducing some signal distortion at the system output. Because in many cases this minor distortion will not be objectionable, we shall not concern ourselves with it at this point.

A Wiener solution is obtained only in the limit as the speed of adaptation is brought to zero, i.e. as  $\mu$  is brought to zero. The weight dynamics that are inherent in adaptation give rise to "non-Wiener" effects that cause signal cancellation. These effects are the central concern of this paper.

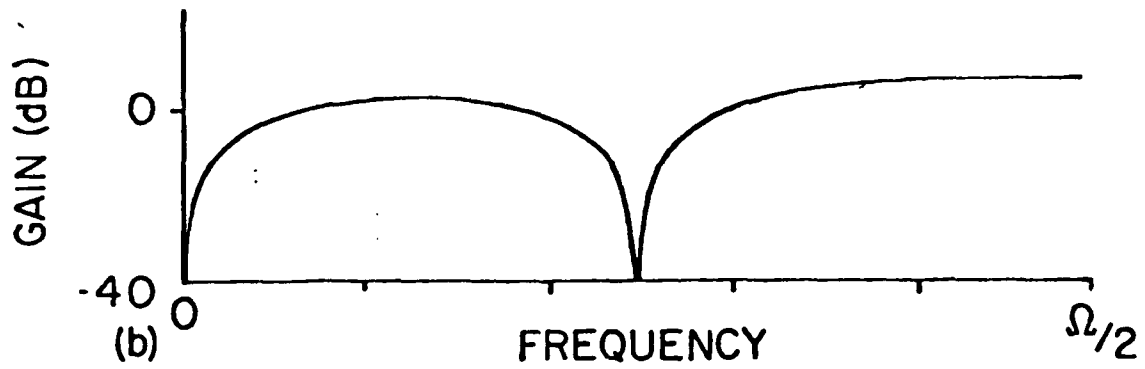
If, as we have assumed, the signal components in the reference input are of low power compared to that of the jammer components, we can neglect effects of the signal at the input to the adaptive filter. Assume that the jammer is sinusoidal. The sinusoidal input to the adaptive filter then causes a situation like that represented in Fig. 2. The signal flow path from primary input to system output behaves like a notch filter. Thus, both jammer components and signal components at and around the jammer frequency will be notched at the system output. Notching is a non-Wiener effect.

An experiment was conducted to confirm the behavior just described. A Howells-Applebaum sidelobe canceller was configured with two omni-directional elements placed  $1/4$  wavelength apart, and with four weights in the adaptive filter. A bandpass signal was selected with a center frequency at one quarter of the sampling frequency, with a bandwidth of 20%, and with broadside incidence. A sinusoidal jammer was chosen with a frequency of one quarter the sampling frequency, a power of 100, and an incidence angle of 45 degrees off broadside. Figure 7 shows the antenna pattern and frequency response after convergence. The sidelobe canceller appears to be functioning in the manner described above. Figures 7(a) and 7(b) show that a -40 dB null has been formed in the jammer direction at the jammer frequency. Figure 7(c) shows that the antenna's frequency response in the signal direction is reasonably flat over the signal bandwidth.

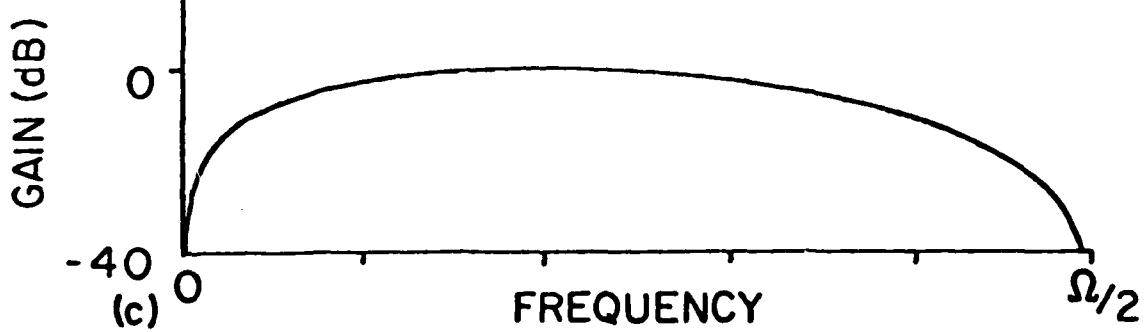
BANDPASS SIGNAL  
POWER = 1.0



(a)



(b)



(c)

Fig. 7. Behavior of "converged" Howells-Applebaum sidelobe canceller.  
(a) Antenna pattern plotted at jammer frequency. (b) Frequency response in jammer direction. (c) Frequency response in signal direction.

Overall, Fig. 7 indicates that the Howells-Applebaum sidelobe canceller is working perfectly.

However, observations of the antenna output spectra indicate otherwise. Figure 8 shows an ensemble average of the signal, jammer, and antenna output spectra. The sidelobe canceller was operated with a  $\mu$  of  $2.5 \times 10^{-4}$ . The non-Wiener notch effect and the Wiener signal distortion inherent in this simple system are evident from Figure 8(c). The notch will always be present, and it can be narrowed only by slowing the rate of adaptation.

#### VI. SIGNAL CANCELLATION PHENOMENA IN FROST ADAPTIVE BEAMFORMERS

Frost's original conception of an adaptive beamformer is shown in Fig. 9. Beam steering delays are inserted in the usual manner to set the look direction at any desired angle. The frequency response of the array to signals arriving in the look direction is equivalent to that of a transversal filter whose weights are the sums of the columns of weights of the actual beamformer. Therefore, during adaptation, the weights are varied to minimize output power while sustaining sums of columns of weights at prescribed values to achieve the specified frequency response in the look direction. Otherwise, minimizing output power would simply cause all the weights to collapse to zero.

Except for the freedom from signal distortion inherent in its constrained Wiener solution, the Frost beamformer shows the same signal cancellation effects that were observed with the Howells-Applebaum sidelobe canceller. To investigate these effects, another experiment was conducted using a four-element Frost array having four weights per element. A signal with 20% bandwidth and center frequency equal to one quarter of the sampling frequency was generated to be incident from broadside. The constraint in the look direction was set to unit gain and zero phase from zero frequency to half the sampling rate, i.e. to a flat response over all frequencies. The jammer was sinusoidal at

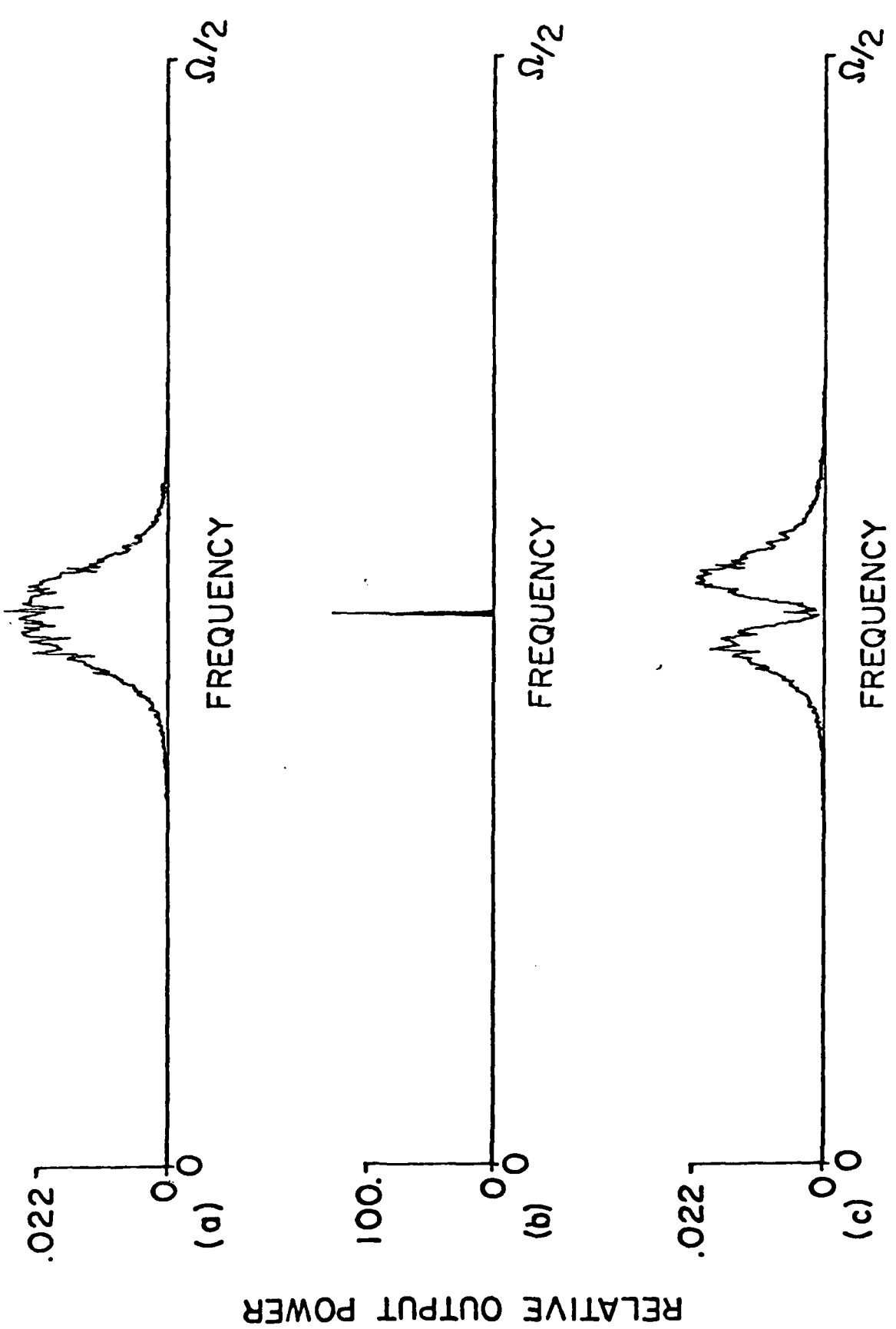


Fig. 8. Power spectra of Howells-Applebaum beamformer simulation.  
 (a) Input signal spectrum. (b) Jammer spectrum.  
 (c) Beamformer output spectrum.

# EQUIVALENT LOOK-DIRECTION FILTER

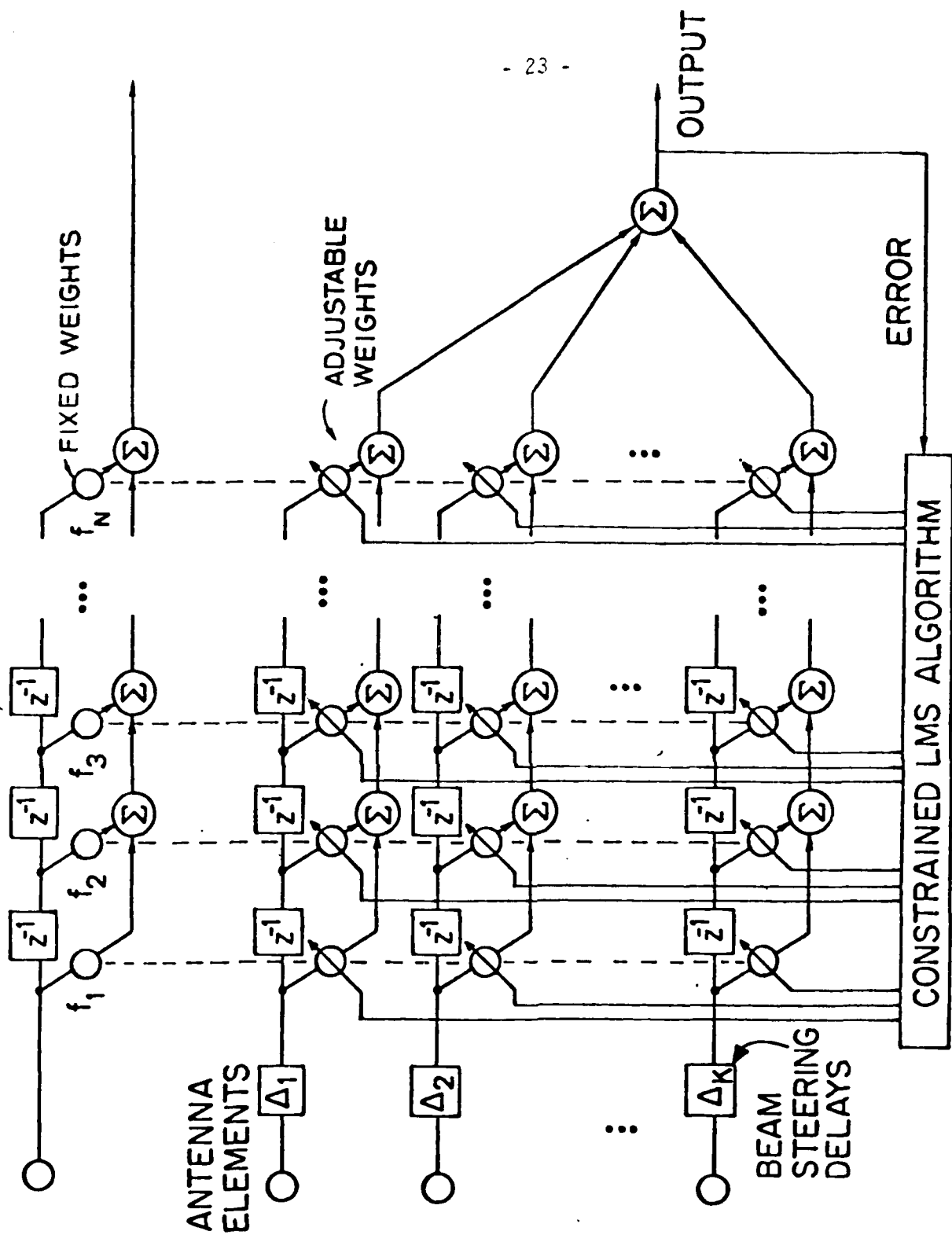


Fig. 9. Frost beamformer and equivalent look-direction filter.

one quarter the sampling frequency. In these experiments, ambient noise and receiver noise were negligible. Figure 10 shows the converged antenna pattern and the frequency response plots in both the signal and jammer directions. Observe that the look-direction gain is flat and the gain in the jammer direction is quite small; it was measured at 40 dB below the main beam gain. As in the Howells-Applebaum sidelobe canceller, the antenna pattern indicates that the beamformer is working perfectly.

The bandpass signal whose spectrum is shown in Fig. 11(a) was received by this adaptive beamformer. The spectrum of the sinusoidal jammer is shown in Fig. 11(b). Figure 11(c) shows the output signal spectrum of the Frost beamformer operating with a  $\mu$  of  $10^{-3}$ . The input signal appears at the output, having gone through a notch filter. The notching effect evident in the output signal spectrum is indicative of gross signal distortion at the beamformer output. The notch width is not exactly equal to the reciprocal of the learning curve time constant, but exceeds it by a factor of 2. The conditions for the derivation of the notch width formula (24), i.e., sinusoidal signals appearing with exact 90° separation at the inputs to the two weights, are not met with the 16-weight Frost processor under the above stated experimental conditions. Nevertheless, the simple formula (24) does give at least an approximate prediction of notch width that is applicable at most jammer angles.

The notching phenomena in the Frost beamformer are somewhat more complicated than those in adaptive noise cancelling systems. The form of the Frost beamformer shown in Fig. 9 is not the simplest one for the study of signal notching phenomena. For this purpose, we have used a more suitable form of Frost beamformer, developed by Griffiths and Jim [17], and shown in Fig. 12.

The realization of Fig. 12 can be understood as follows. The filter containing fixed weights determines the frequency response in the look direction. The look-direction fre-

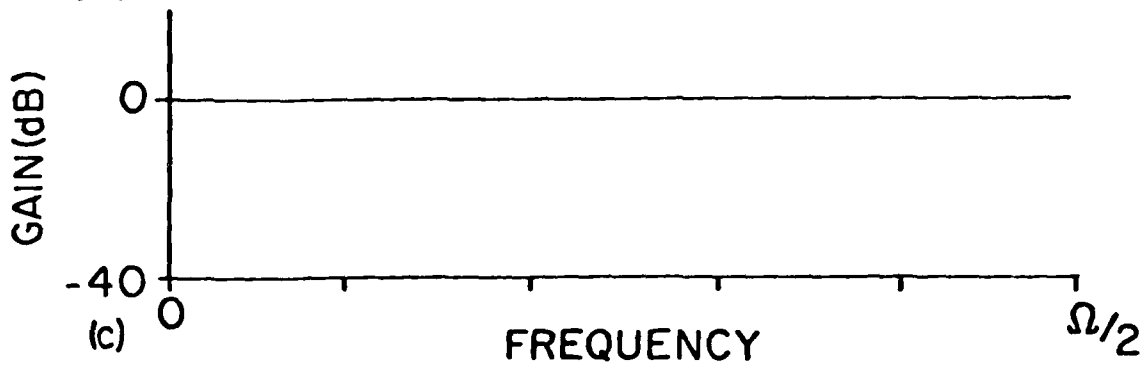
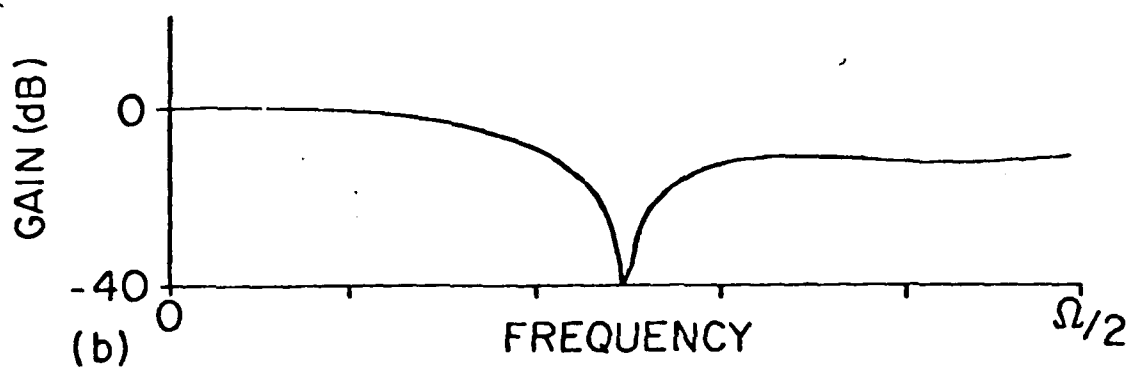
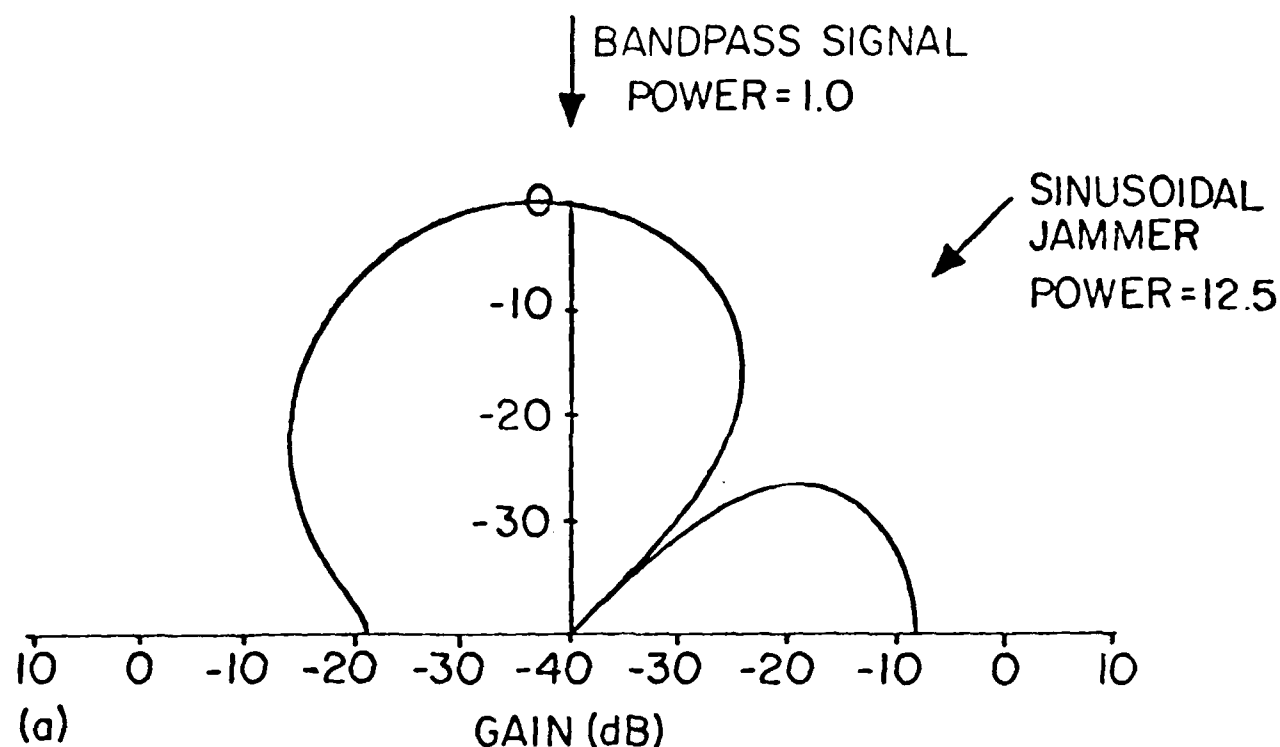


Fig. 10. Behavior of "converged" Frost beamformer. (a) Antenna pattern plotted at jammer frequency. (b) Frequency response in jammer direction. (c) Frequency response in signal direction.

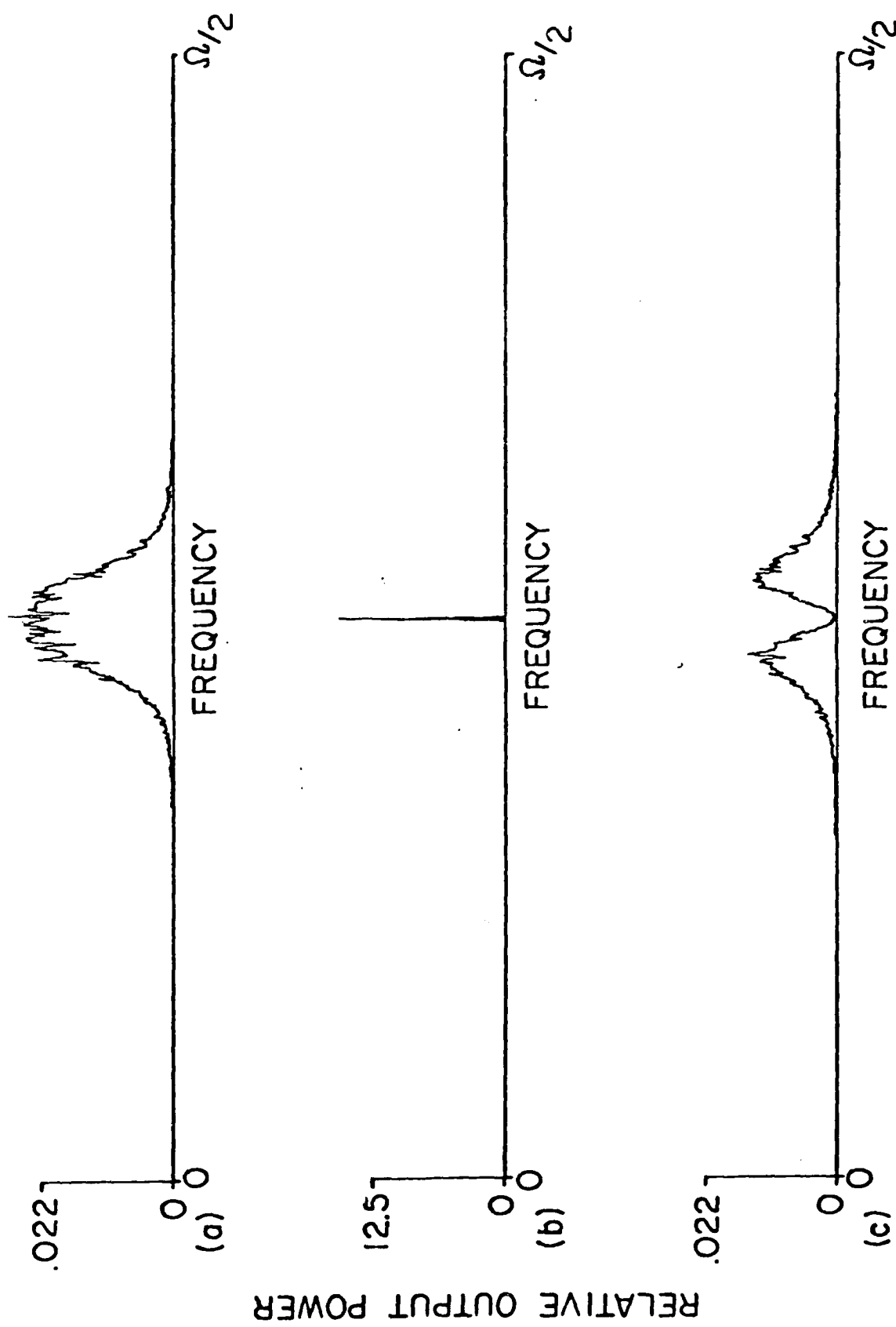


Fig. 11. Power spectra of Frost beamformer simulation. (a) Input signal spectrum.  
 (b) Jammer spectrum. (c) Beamformer output spectrum.

LOOK-DIRECTION FILTER

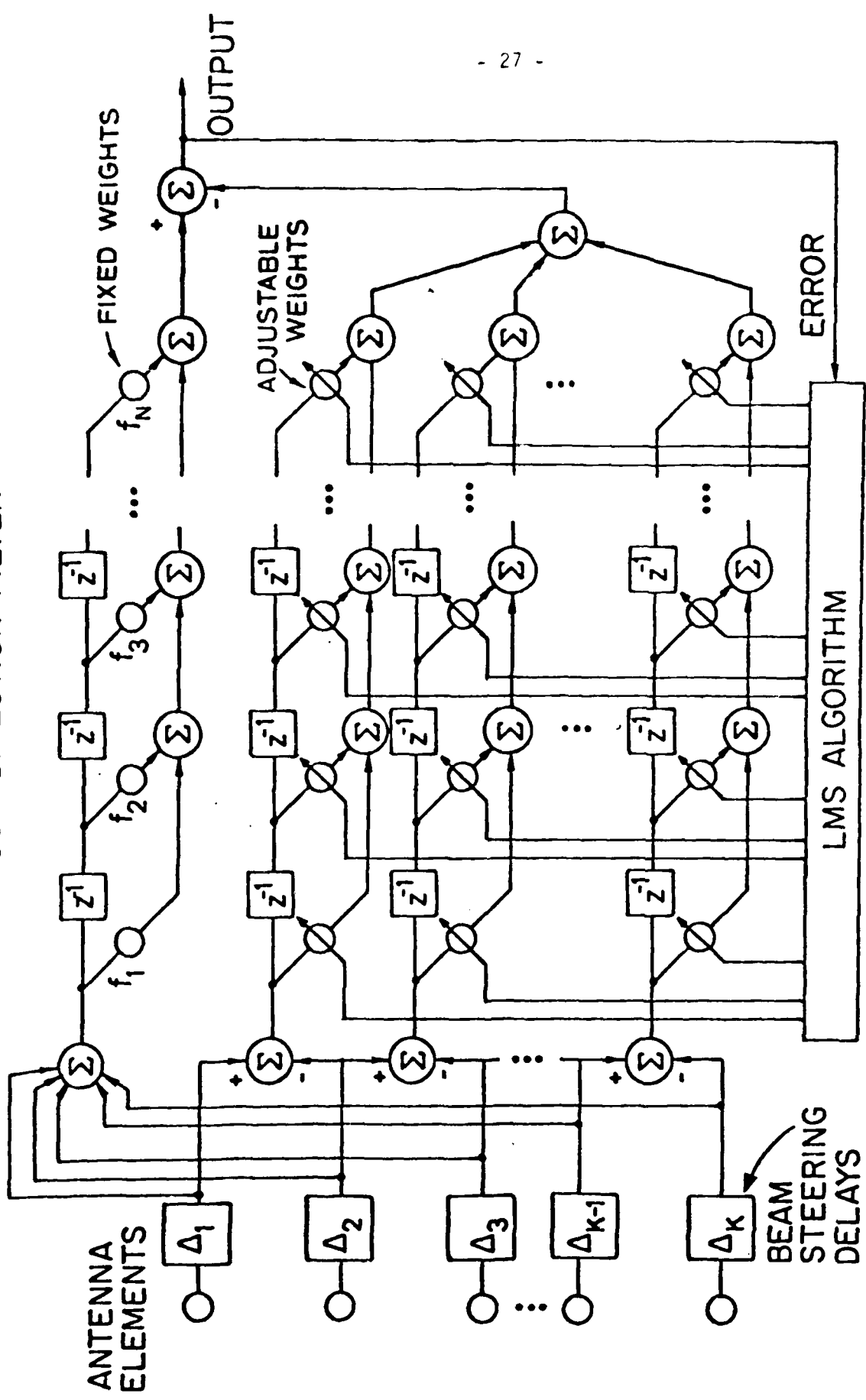


Fig. 12. Griffiths/Jim realization of the Frost adaptive beamformer.

quency response is unaffected by the multichannel adaptive filter since the subtractive preprocessor has removed all look-direction signal components from the filter inputs. Adjusting the weights to minimize output power is tantamount to minimizing output power subject to a response constraint in the look direction. If  $K$  is the number of antenna elements, the Frost constraint reduces the number of degrees of freedom by the factor  $\frac{K-1}{K}$ .

For the sake of discussion, let the look direction constraint be unit gain and zero phase over all frequencies. Referring to Fig. 12, this would correspond to  $f_1=1$  and  $f_2=f_3=\dots=f_K=0$ . The useful signal arriving in the look direction encounters a unit gain with the main beam so constrained. This is analogous to the direct primary signal path shown in Fig. 1. A jammer signal arriving at other than the look direction encounters an adaptive filter, analogous to the reference signal path shown in Fig. 1. A sinusoidal jammer off the look direction therefore causes sinusoidal fluctuations in all the weights, which creates a notch along the primary signal flow path to the output via the fixed weight filter. Notching phenomena in this system are very much like those of the adaptive canceller shown in Fig. 1. Look-direction signals do not appear at the adaptive filter inputs; only interference is present there. Both signal and jammer are present in the primary signal flow path, and both signal and jammer experience notching at the jammer frequency. With high speed adaptation, the notch could be very wide, incurring the risk of losing the signal in the jammer cancellation process, in effect "throwing the baby out with the bath water."

To further explore the signal cancellation problem, additional experiments were conducted with the Frost beamformer. The jammer was again sinusoidal, while the look-direction signal was composed of white noise of unit power. The jammer power was varied. Spectra of the beamformer outputs are shown in Fig. 13. With the jammer

power set at its lowest level, the signal cancellation notch is at its smallest bandwidth, as indicated in Fig. 13(a). As the jammer power is increased, keeping all other parameters constant, the notch width increases. Figure 13(c) shows the widest notch for the strongest jammer signal that was applied. In all of the illustrated cases, the relationship between notch width and reciprocal adaptive time constant has been preserved.

Figure 14 shows the results of yet another experiment with the Frost beamformer. Here the signal was white, and the jammer was a strong bandpass noise. Signal components were partially cancelled over the entire jammer spectral band, corresponding to extensive signal distortion. Results of this type occur only in cases of very rapid adaptation. For the Fig. 14 experiment, the time constant of the adaptive process was approximately equal to 20 sampling periods. The bandwidth of the jammer was approximately equal to 5% of the center frequency.

To this point, the discussion has centered upon the effects of signal cancellation. Attention will now be given to two remedies for the problem. The first is a method devised by K. Duvall based on the use of two signal processing systems, one to perform the adaptation, the other to generate the system output signal.

## VII. THE DUVALL BEAMFORMER

The signal cancellation effects that have just been illustrated are due to interaction between the signal and the jammer in the adaptive beamformer. Since interaction is the root of the problem, it is useful to consider beamformer structures that separate the signal and the jammer in the adaptive beamformer. A system based on this rationale is shown in Fig. 15a.

This system makes use of two beamformers. The beamformer on the right is connected directly to the elements and is used to derive the array output signal. It is, how-

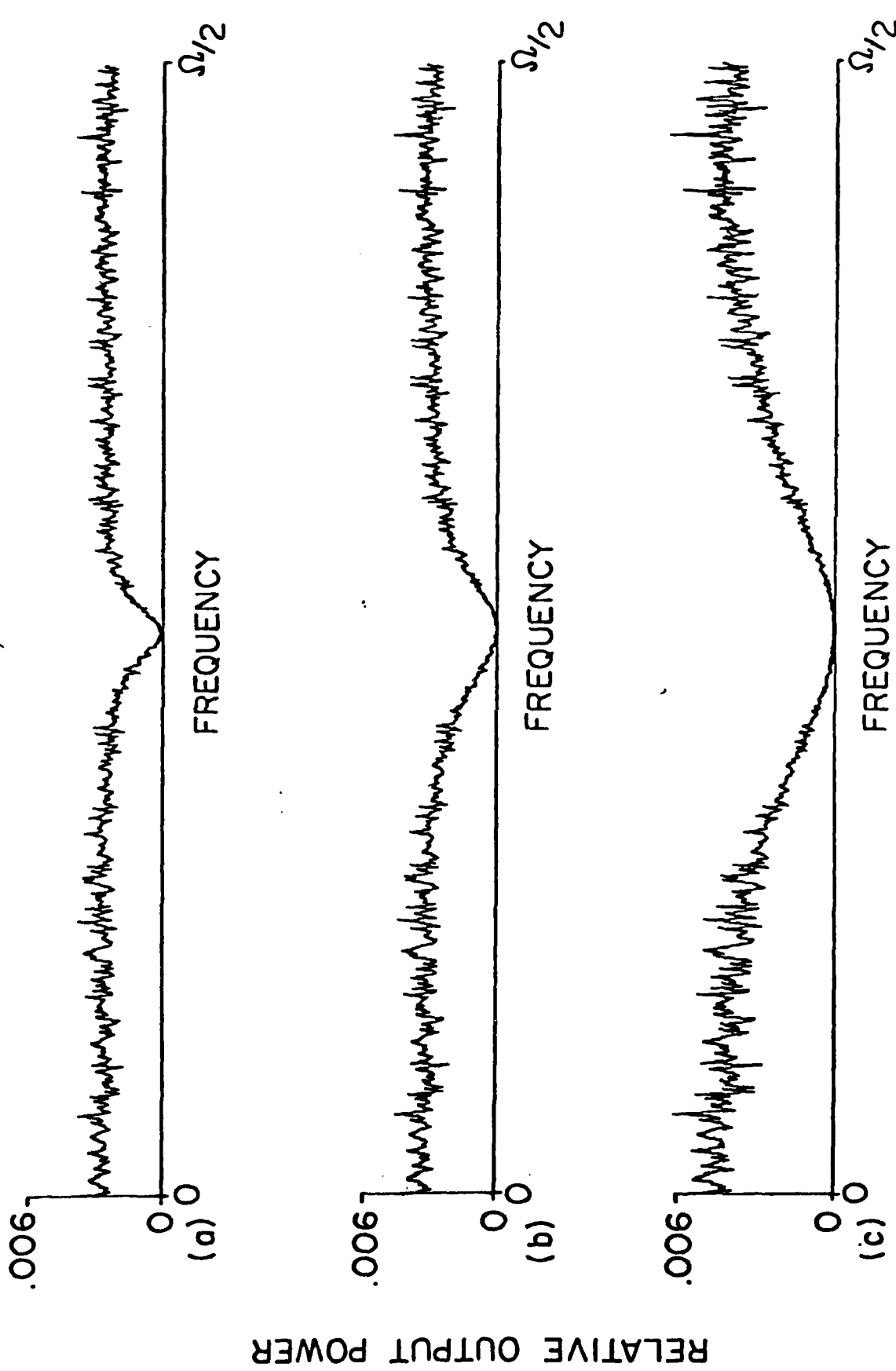


Fig. 13. Frost beamformer output spectra for white-noise signal of power 1.0 and sinusoidal jammer. (a) Jammer power = 12.5. (b) Jammer power = 25.0. (c) Jammer power = 50.0.

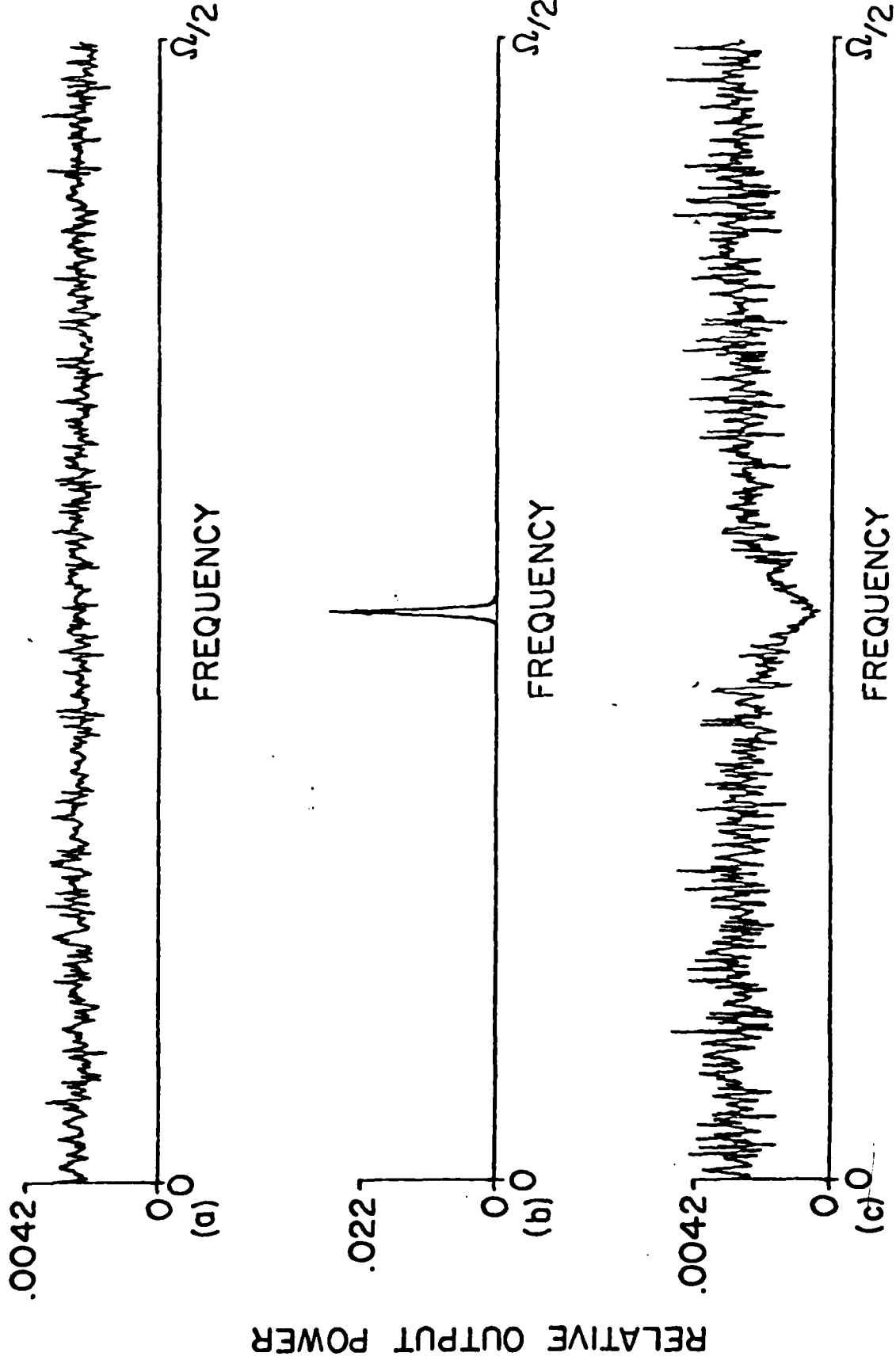


Fig. 14. Power spectra of Frost beamformer simulation with white-noise signal and wide-band jammer. (a) Jammer spectrum. (b) Input signal spectrum. (c) Beamformer output spectrum.

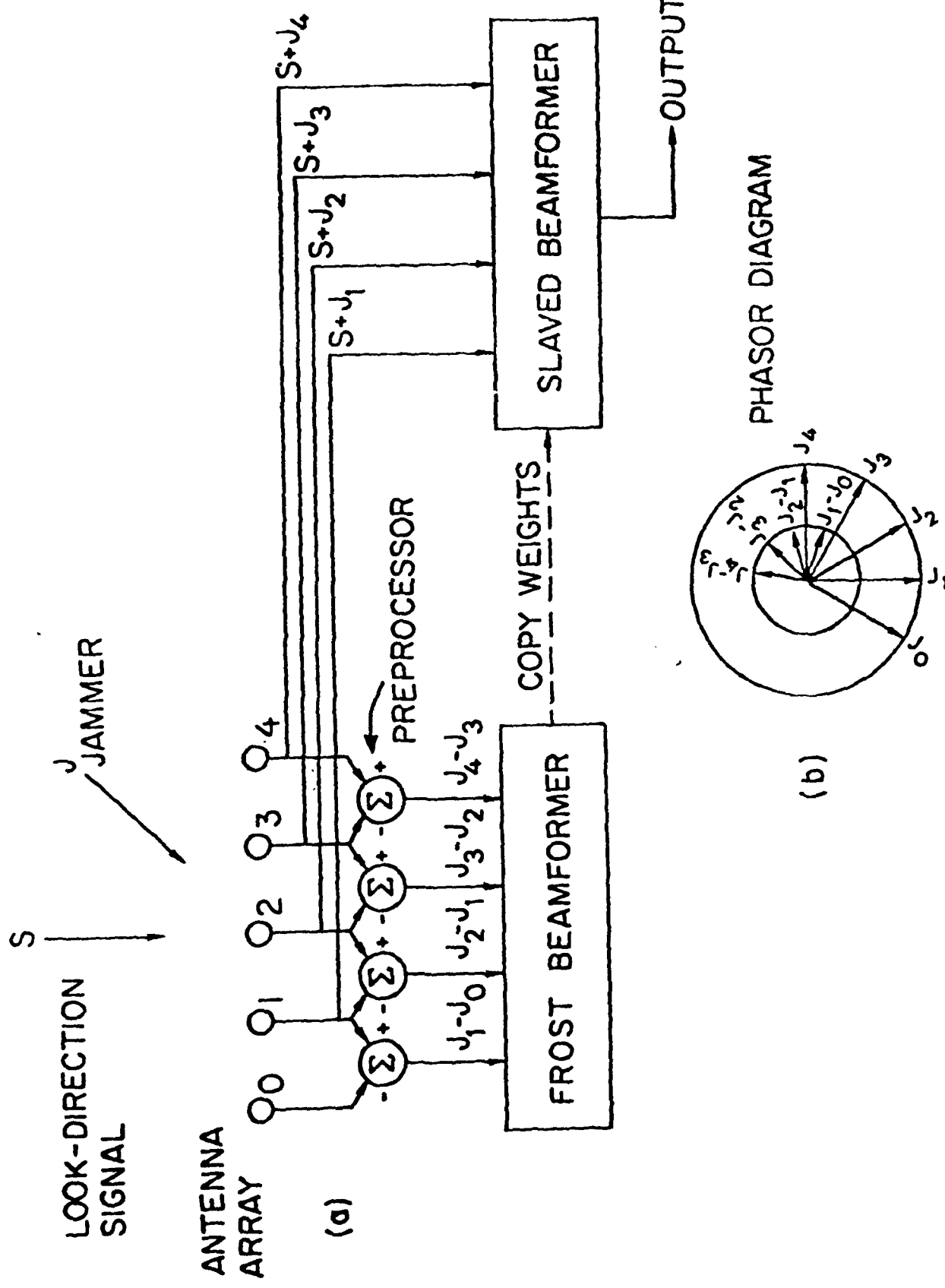


Fig. 15. Duvall beamformer for eliminating cancellation jamming. (a) Block diagram of the beamformer. (b) phasor diagram showing inputs and outputs of preprocessor.

ever, a slaved beamformer rather than the adaptive beamformer that would usually be expected in this position. The beamformer on the left is a Frost adaptive beamformer connected to the array elements through a subtractive preprocessor. The preprocessor excludes the look-direction signal from this beamformer, but admits jammer signals in a modified form. The adaptive beamformer generates a set of weights that provides some specified look-direction gain (given by the Frost constraints) while minimizing (in the least-squares sense) the jammer contribution. These weights are copied into the slaved beamformer to provide the desired signal reception and jammer rejection.

The crucial point here is the relationship between the jammer signals in the two beamformers. The phasor diagram shown in Fig. 15b helps to clarify this issue. The jammer components received by the antenna elements are indicated by a set of equal-amplitude, uniformly spaced phasors  $J_0$ ,  $J_1$ ,  $J_2$ ,  $J_3$ , and  $J_4$ . The phasor inputs to the Frost beamformer are  $J_1-J_0$ ,  $J_2-J_1$ ,  $J_3-J_2$ , and  $J_4-J_3$ . These, too, are equal-amplitude phasors with the same phase-angle separations as the received jammer components. Since the relative phase angles are the same for the jammer components in both beamformers, correct alignment of the jammer null in the Frost beamformer assures correct alignment of the null in the slaved beamformer. Copying the weights will cause the slaved processor to have a main beam (resulting from the Frost constraints) which is orthogonal to the line of the array, and to have a null in the exact direction of the jammer  $J$ . Note that although the phasor argument applies only to one jammer at one frequency, linearity and superposition show that the principle is applicable to multiple jammers and to broadband as well as narrowband jammers.

The beamformer block diagram shown in Fig. 15a has been simplified, or specialized in certain respects, to facilitate discussion. Beam steering is not shown, but can be accomplished by including steering delays for broadband processes, or phase shifters for

narrowband processes, behind each array element. The Frost algorithm can be applied, as shown, or any of a number of constrained adaptive algorithms that have appeared in the literature. It is very straightforward, for example to apply Widrow's pilot-signal algorithm in this system. Generalization of the subtractive preprocessor is also possible. C. W. Jim has described a class of spatial filters in [17] that offers greater flexibility than is shown in Fig. 15a.

Experiments have been performed with this system, with results given in Figs. 16 and 17. Figure 16 compares the output spectrum of the Frost beamformer (Fig. 16d) with that of a Frost-based Duvall beamformer (Fig. 16c), both adapting with a time constant of approximately 20 samples, with the same array and with the same signal and jammer. The array and jammer are the same as in the experiment described in section VI. After the comparative experiments were performed, the Frost beamformer showed evidence of strong signal cancellation, while the Duvall beamformer showed no evidence of signal cancellation. In the time domain, Fig. 17 compares the look-direction input signal with the output signals of the Frost and Duvall beamformers. In both cases the weights were initialized to zero, and adaptive transients are visible at the beginnings of the output tracings. Beyond the region where the transient exists, signal distortion is present in the Frost beamformer output (Fig. 17c). The distortion power was measured to be 6 dB below the input signal power. Such distortion is not apparent at the output of the Duvall beamformer (Fig. 17b). Here the distortion was measured to be 110 dB below signal level.

The Duvall beamformer appears to be an important development toward mitigating the effects of signal cancellation. The concept is new, however, and possible limitations on its performance have not yet been fully assessed. Effects of component inaccuracies and array imperfections are not yet understood. Alternative techniques for steering nulls

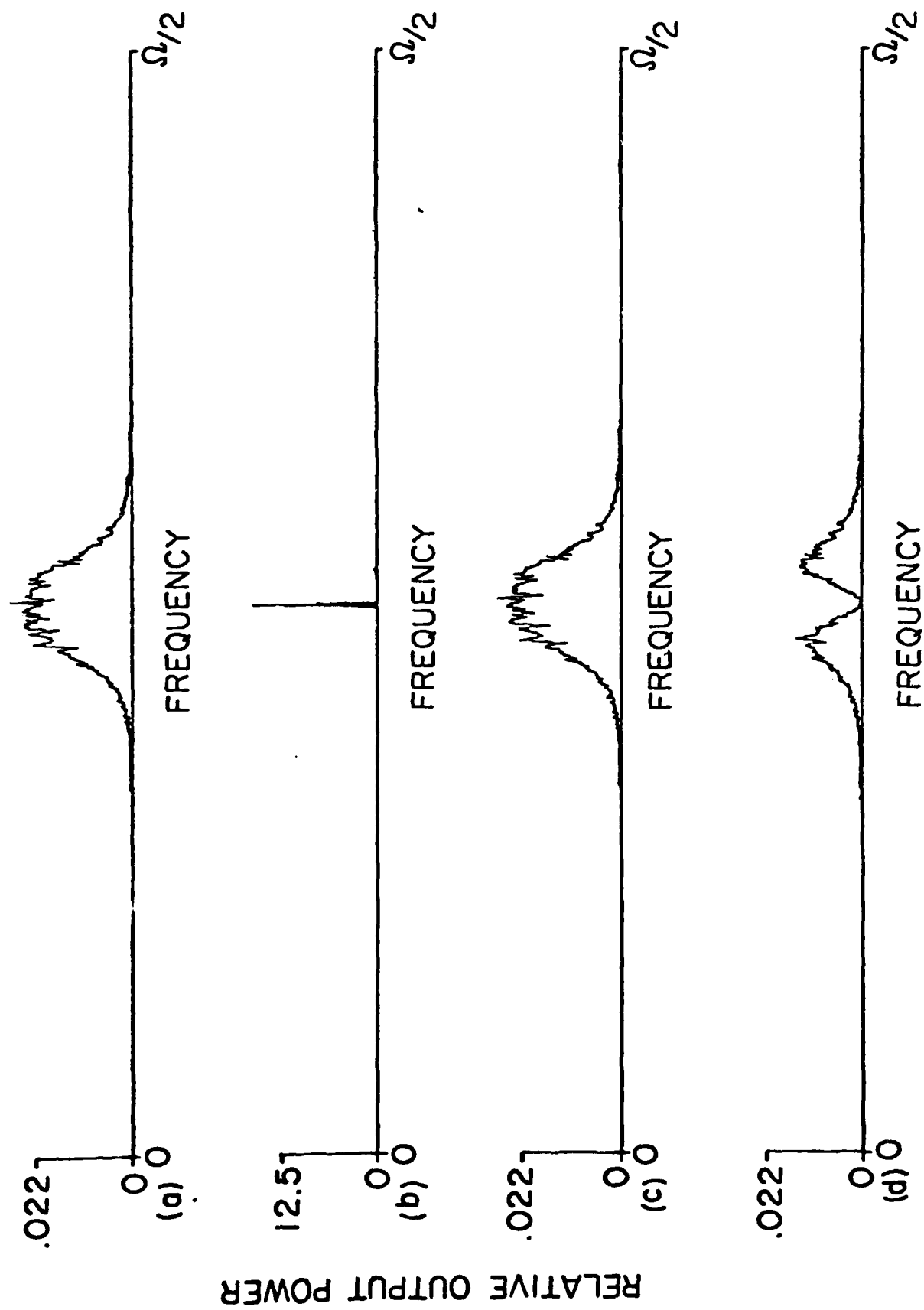


Fig. 16. Comparison of Frost and Duval beamformers. (a) Input signal spectrum. (b) Jammer spectrum.  
(c) Duval beamformer output spectrum. (d) Frost beamformer output spectrum.

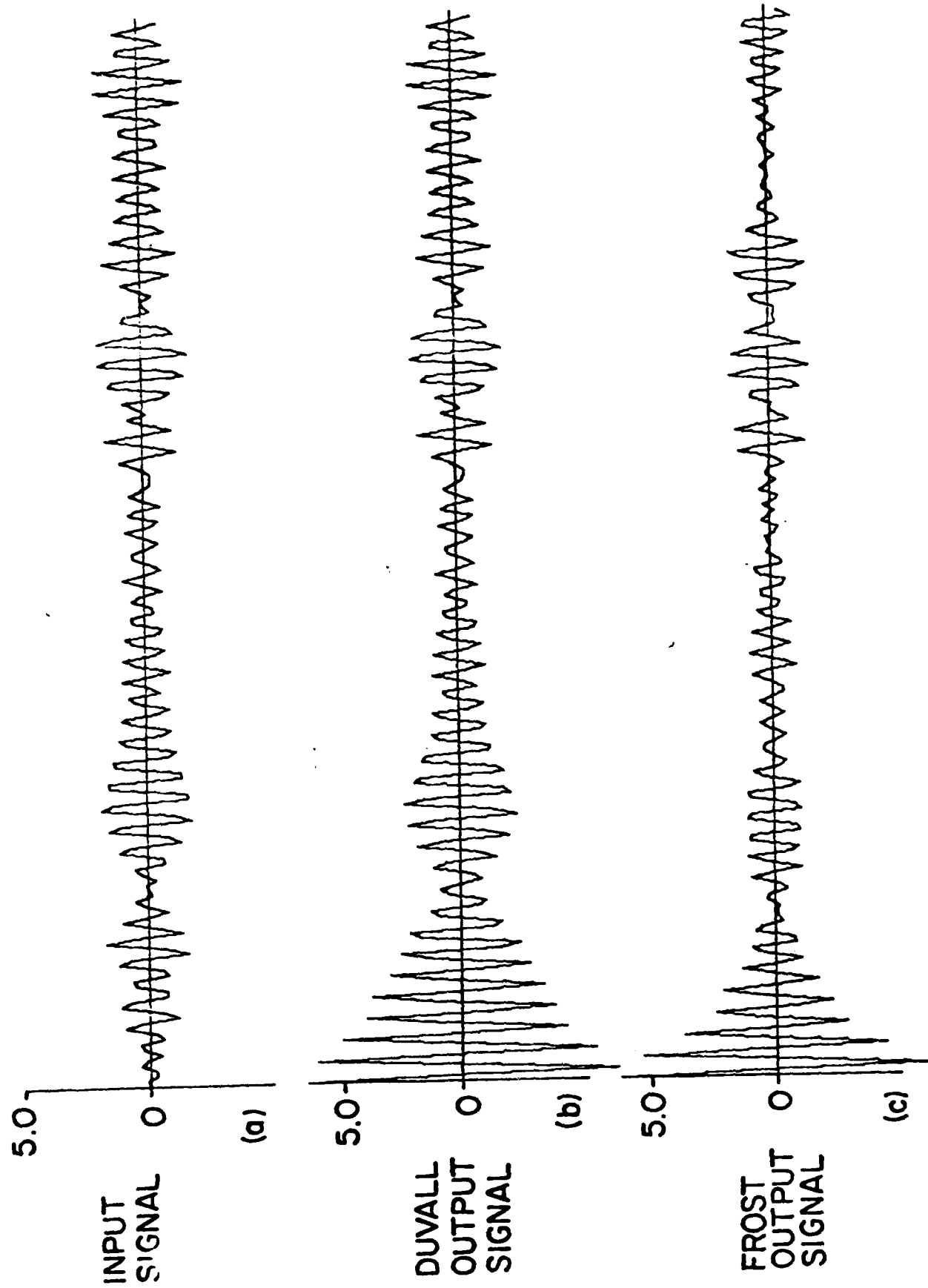


Fig. 17. Comparison of time-domain outputs of Frost and Duvall beamformers. (a) Signal input.  
(b) Duvall beamformer output. (c) Frost beamformer output.

in the look direction have not been examined in detail, and various performance measures remain to be studied. Other methods for eliminating or reducing signal cancellation effects are also being pursued, such as spatial dither algorithms.

### VIII. SPATIAL DITHER ALGORITHMS

Spatial dither algorithms have been conceived for the purpose of applying locally controlled modulation to signals arriving at angles other than the look direction, while leaving inputs from the look direction unmodulated and undistorted. The effect is to cause jammers arriving off the look direction to be spread spectrally, thereby reducing jammer power density. When used with a conventional adaptive beamformer, spatial dither reduces signal cancellation effects. The same process has the additional capability of modulating a "smart" jammer signal in a way that is totally unpredictable to the jammer, thus in many cases rendering it "less smart."

A conceptually simple form of spatial dither algorithm is the "3/4-inch plywood" approach, pictured in Fig. 18. The elements of an antenna array can be imagined to be fixed to a piece of plywood that provides a rigid support, so that the entire array can be moved mechanically. In either one or two dimensions, the array is moved in directions which are orthogonal to the look direction. Far-field emanations arriving from the look direction will be undistorted by the mechanical motion, while emissions from sources off the look direction will be distorted by an unusual shift-of-time-base form of modulation. Electronic means of implementing this spatial dither process are being devised.

The outputs of the antenna elements of Fig. 18 could be applied to a time delay and sum (nonadaptive) beamformer, to a conventional adaptive beamformer, or to a Duvall adaptive beamformer. Spatial dither could be beneficial in each case. By reducing jammer power density, some anti-jam protection is provided without adaptive beamforming, and additional anti-jam protection is provided with adaptive beamforming.

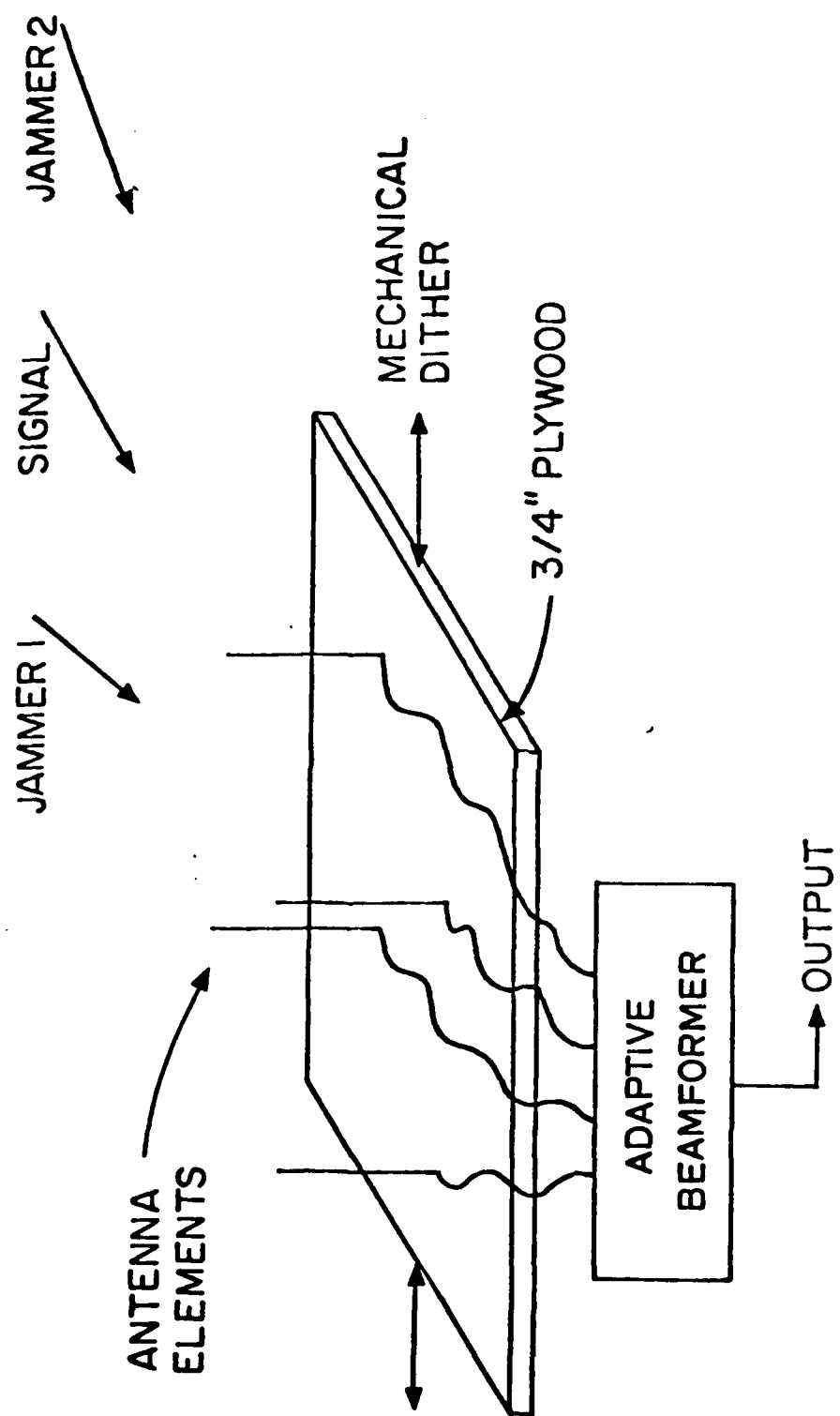


Fig. 18. Mechanical spatial dither algorithm ("3/4-inch plywood" approach) for a small antenna array.

The signal cancellation effect can be reduced in a Frost beamformer by using spatial dither preprocessing. Breakup of jammer signal structure is a possible form of signal preprocessing applicable to all types of adaptive and nonadaptive beamformers.

The 3/4-inch plywood approach has been computer simulated, with the results presented in Fig. 19. The motion was random and was executed along a line perpendicular to the look direction. At every 20<sup>th</sup> sample time, the plywood position was changed; the new position was drawn randomly from a uniform distribution ranging from zero to 11.2 wavelengths. Figure 19(a) shows the spectrum of the look-direction input signal, in this case a bandpass signal. The sinusoidal jammer spectrum is shown in Fig. 19(b). The spectrum of the jammer from the physical reference frame of the array is shown in Fig. 19(c). It is clear that the jammer power is greatly spread, that jammer power density is significantly reduced, and that the jammer signal is severely distorted from its original form. In the simulation, bandpass filters were used with each antenna output to represent the effects of a receiver. The filtered signals were then applied to a conventional Frost adaptive beamformer. Some signal distortion is evident, but the amount of distortion is greatly reduced by the spatial dither. The output spectrum shown in Fig. 19(d) is far less distorted than that of Fig. 10(c), a comparable spectrum obtained without spatial dither.

## IX. CONCLUSION

Signal cancellation effects occur in conventional adaptive beamformers when jammer power and adaptation rates are high. These effects can cause signal loss in the case of narrowband signals, or cause significant signal distortion in the case of wideband signals. Means of combating signal cancellation have been proposed, namely the Duvall beamformer and the spatial dither algorithm. The latter approach will probably not be as effective as the former against signal cancellation but has the capability of scrambling

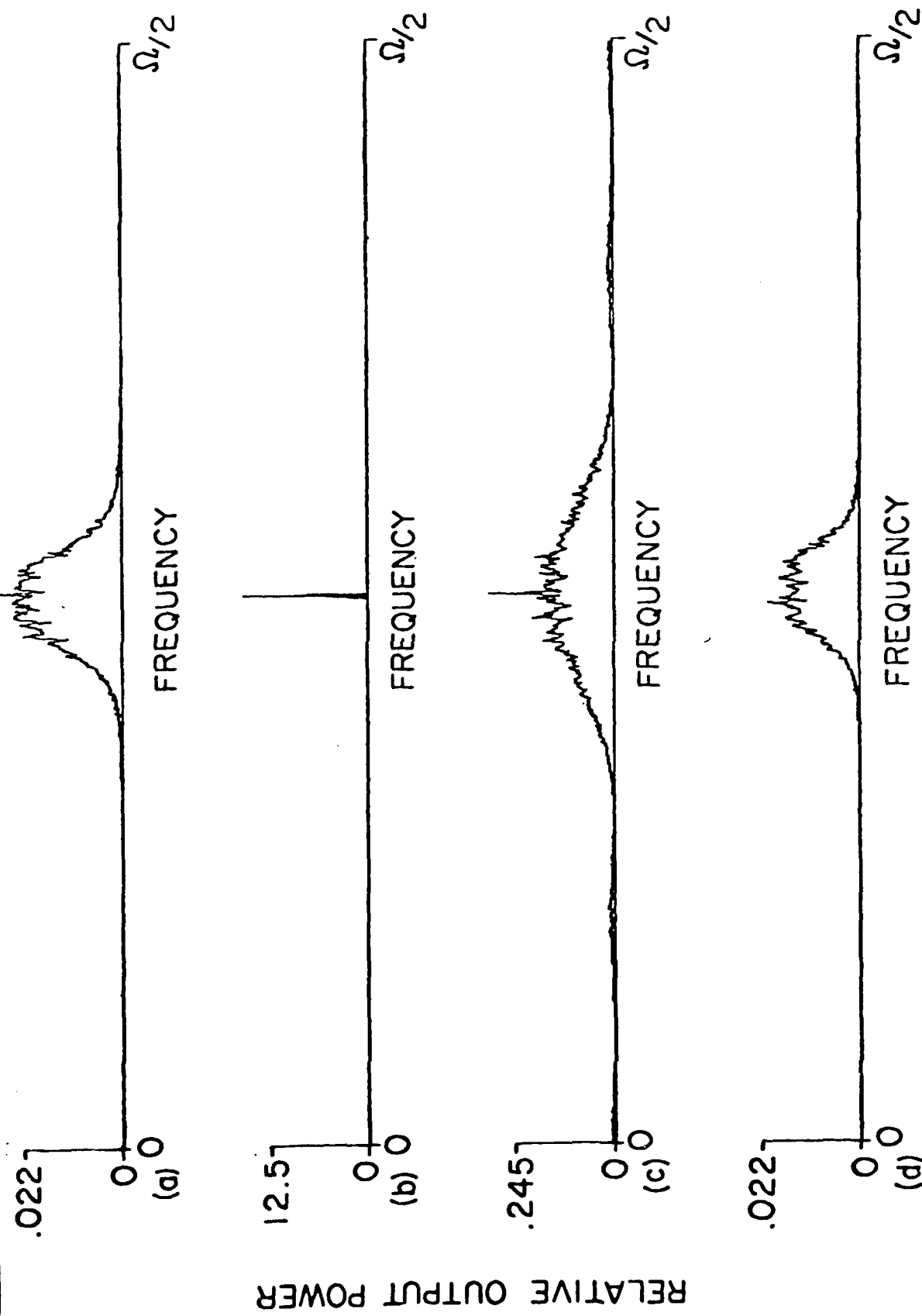


Fig. 19. Input and output power spectra of Frost beamformer with spatial dither preprocessing.  
(a) Input signal spectrum. (b) Undithered jammer spectrum. (c) Dithered jammer spectrum.  
(d) Adaptive array output spectrum.

"smart" jammer signals.

## REFERENCES

1. Howells, P., "Intermediate Frequency Side-Lobe Canceller," U. S. Patent 3202 990, Aug. 24, 1965.
2. Special Issue on Adaptive Antennas, IEEE Transactions on Antennas and Propagation, Vol. AP-24, No. 5, Sept. 1976.
3. Gabriel, W. F., "Adaptive Arrays--An Introduction," Proc. IEEE, vol. 64, pp. 239-272, Feb. 1976.
4. Widrow, B., "Adaptive Antenna Systems," Proceedings of the IEEE, Vol. 55, No. 12, pp. 2143-2159, Dec. 1967.
5. Griffiths, L. J., "A Simple Adaptive Algorithm For Real-Time Processing In Antenna Arrays," Proceedings of the IEEE, Vol. 57, No. 10, pp. 1696-1704, Oct. 1969.
6. Frost, III, O. L., "An Algorithm For Linearly Constrained Adaptive Array Processing," Proceedings of the IEEE, Vol. 60, No. 8, pp. 928-935, Aug. 1972.
7. Zahm, C. L., "Applications of Adaptive Arrays to Suppress Strong Jammers in the Presence of Weak Signals," IEEE Transactions on Aerosp. Electron. Systems, Vol. AES-9, pp. 260-271, 1973.
8. Compton, R. T., Jr., R. J. Huff, W. G. Swarner, and A. A. Ksienki, "Adaptive Arrays for Communication Systems: An Overview of Research at the Ohio State University," IEEE Trans. on Ant. and Prop., Vol. AP-24, No. 5, pp. 599-606, Sept. 1976.

9. Compton, R. T., Jr., "An Experimental Four-Element Adaptive Array," IEEE Trans. on Ant. and Prop., Vol. AP-24, No. 5, pp. 697-706, Sept. 1976.
10. Brennan, L. E. and I. S. Reed, "Convergence Rate in Adaptive Arrays," Technology Service Corp., Rept. No. TSC-PD-177-4, Jan. 13, 1978.
11. White, W. D., "Adaptive Cascade Networks for Deep Nulling," IEEE Trans. on Ant. and Prop., Vol. AP-26, No. 3, pp. 398-402, May 1978.
12. Widrow, B. et al., "Adaptive Noise Cancelling: Principles and Applications," Proceedings of the IEEE, Vol. 63, No. 12, pp. 1692-1716, Dec. 1975.
13. Glover, J., (Ph.D. dissertation), "Adaptive Noise Cancelling of Sinusoidal Interference," Stanford Electronics Laboratories, Stanford University, Dec. 1975.
14. Glover, J., "Adaptive Noise Cancelling Applied to Sinusoidal Interferences," IEEE Transactions on Acoustics, Speech and Signal Processing, Vol. ASSP-25, No. 6, pp. 484-491, Dec. 1977.
15. Widrow, B., and M. E. Hoff, Jr., "Adaptive Switching Circuits," IRE WESCON Conv. Rec., pt. 4, pp. 98-104, 1960.
16. Widrow, B., et al., "Stationary and Nonstationary Learning Characteristics of the LMS Adaptive Filter," Proceedings of the IEEE, Vol. 64, No. 8, pp. 1151-1162, Aug. 1976.
17. Jim, C. W., "A Comparison of Two LMS Constrained Optimal Array Structures," Proceedings of the IEEE, Vol. 65, No. 12, pp. 1730-1731, Dec. 1977.